Int J Earth Sci (Geol Rundsch) (2006) 95: 1019–1037
DOI 10.1007/s00531-006-0082-x

ORIGINAL PAPER

P. Tropper · I. Deibl · F. Finger · R. Kaindl

# *P–T–t* evolution of spinel–cordierite–garnet gneisses from the Sauwald Zone (Southern Bohemian Massif, Upper Austria): is there evidence for two independent late-Variscan low-*P*/high-*T* events in the Moldanubian Unit?

Received: 22 April 2005 / Accepted: 3 February 2006 / Published online: 22 April 2006


**Abstract** The Sauwald Zone, located at the southern rim of the Bohemian Massif in Upper Austria, belongs to the Moldanubian Unit. It exposes uniform biotite + plagioclase ± cordierite paragneisses that formed during the post-collisional high-*T*/low-*P* stage of the Variscan orogeny. Rare metapelitic inlayers contain the mineral assemblage garnet + cordierite + green spinel + sillimanite + K-feldspar + plagioclase + biotite + quartz. Mineral chemical and textural data indicate four stages of mineral growth: (1) peak assemblage as inclusions in garnet (stage 1): garnet core + cordierite + green spinel + sillimanite + plagioclase ($An_{35–65}$); (2) post-peak assemblages in the matrix (stages 2, 3): cordierite + spinel (brown-green and brown) ± sillimanite ± garnet rim + plagioclase ($An_{10–45}$); and (3) late-stage growth of fibrolite, muscovite and albite ($An_{0–15}$) during stage 4. Calculation of the *P–T* conditions of the peak assemblage (stage 1) yields 750–840°C, 0.29–0.53 GPa and for the stage 2 matrix assemblage garnet + cordierite + green spinel + sillimanite + plagioclase 620–730°C, 0.27–0.36 GPa. The observed phase relations indicate a clockwise *P–T* path, which terminates below 0.38 GPa. The *P–T* evolution of the Sauwald Zone and the Monotonous Unit are very similar, however, monazite ages of the former are younger (321 ± 9 Ma vs. 334 ± 1 Ma). This indicates that high-*T*/low-*P* metamorphism in the Sauwald Zone was either of longer duration or there were two independent phases of late-Variscan low-*P*/high-*T* metamorphism in the Moldanubian Unit.

**Keywords** Moldanubian · Sauwald zone · *P–T–t* path · Variscan orogeny · Cordierite

P. Tropper (✉) · I. Deibl · R. Kaindl
Faculty of Geo- and Atmospheric Sciences,
Institute of Mineralogy and Petrography,
University of Innsbruck, Innrain 52,
Innsbruck 6020, Austria
E-mail: Peter.Tropper@uibk.ac.at
E-mail: Reinhard.Kaindl@uibk.ac.at

F. Finger
Division of Mineralogy and Material Sciences,
University of Salzburg,
Hellbrunnerstrasse 34, III,
Salzburg 5020, Austria

## Introduction

The Devonian-Carboniferous Variscan orogeny of central Europe involves as a special late-stage feature a pervasive low-*P*/high-*T* overprint (Zwart and Dornsiepen 1978; Franke 2000). This Abukuma-style metamorphic overprint can mainly be seen in the Moldanubian core region of the orogen, where it occurred about contemporaneously with the intrusion of large masses of granitoid magmas derived from the lower crust and the lithospheric mantle (Finger et al. 1997). However, even in the middle crust, the temperatures of this low-*P*/high-*T* overprint became so high locally that in significant places partial melting led to the formation of meta- and diatexites.

The causes for this dramatic late-Variscan high heat-flow regime have been repeatedly debated and contrasting geological models have been suggested. Henk et al. (2000) invoke an enhanced heat advection from the mantle, resulting from a late-orogenic delamination of parts of the lower lithosphere. Alternatively, it has been suggested by Gerdes et al. (2000) that the crust was mainly internally heated through significant radiogenic heat production. Finger and Clemens (1995) attribute a great importance to convective heat transport into the middle and upper crustal levels through hot granitoid magmas, whereas O'Brien (2000) considered that upward heat transport also occurred through near-isothermal exhumation of hot granulite bodies.

At the moment, it is quite difficult to critically evaluate and test these various models on a scientific basis because comprehensive petrological information regarding the temporal and spatial *P*–*T* evolution of the Moldanubian crust is missing. Presently, only a few local *P*–*T*–*t* data exist for the low-*P*/high-*T* overprint (Schreyer et al. 1964; Blümel and Schreyer 1976; Linner 1996; Knop et al. 2000; Kalt et al. 2000), where most of the data stem from the Bavarian part of the Moldanubian. For the time being it thus seems to be of great importance to obtain more *P*–*T* data from the Moldanubian low-*P*/high-*T* rocks in various places. In sum, such data will finally lead to a better understanding of the large-scale tectonothermal situation of the Moldanubian Unit within the Variscan orogeny. The present paper should thus be understood as a further mosaic stone in building a comprehensive *P*–*T*–*t* data set of the Moldanubian low-*P*/high-*T* rocks. We present here *P*–*T*–*t* data for a low-*P*/high-*T* region in the Austrian part of the Bohemian Massif, the so-called Sauwald (wild boar forest) Zone in Upper Austria.

## Geological background

It is a widely accepted model that the Variscan orogen resulted from the convergence and final collision of the megacontinents Gondwana and Laurasia, with the intervening microcontinents (Armorican, Avalonian-type terranes) being amalgamated and welded to the Baltic Shield (Franke 2000; Winchester et al. 2002). In the Austrian part of the Bohemian Massif (Fig. 1), the effects of collisional tectonics are best visible in the eastern sector, with the formation and exhumation of the high-*P* granulites of the Gföhl nappe, the thrusting of the Moldanubian Units including the remnants of the oceanic crust (Raabs unit) onto the Moravian foreland plate and a penetrative Barrow-type regional metamorphism at ca. 340 Ma which accompanied this crustal thickening stage (Finger and Steyrer 1995; Fritz et al. 1996). To the west of these Barrow-type metamorphic units (Fig. 1) follows, separated by a fault, a N–S striking paragneiss unit with a late-Variscan low-*P*/high-*T* metamorphic overprint, the so-called Monotonous Unit or Ostrong Unit (Fuchs and Matura 1976). Using various geothermobarometers, Linner (1996) derived *P*–*T* conditions of 690–750°C and 0.4–0.5 GPa for the low-*P*/high-*T* metamorphic peak in the Monotonous Unit. Furthermore, he found relics of higher-pressure minerals such as staurolite and kyanite, showing that the rocks may have evolved along a clockwise *P*–*T* path. U–Pb SHRIMP Monazite ages of 334 ± 1 Ma are thought to date the low-*P*/high-*T* metamorphism in the Monotonous Unit (Friedl 1997). Toward the west, the paragneisses of the Monotonous Unit are intruded by the granitoid generations of the large South Bohemian Batholith, which was implaced between ca. 335 and 300 Ma (Klötzli and Parrish 1996; Friedl 1997; Gerdes et al. 2003). Going further westward, low-*P*/high-*T* metamorphic rocks are again exposed in the Lichtenberg zone, northwest of Linz and in the Sauwald Zone, south of the Danube Fault, as shown in Fig. 1. Most of the rocks in these zones are massive, granitoid looking meta- and diatexites (“Perlgneise”) derived from in situ partial melting of predominantly paragneiss and, to a minor extent, Early Palaeozoic tonalitic–granodioritic gneisses (Frasl and Finger 1991; Friedl et al. 2004). At the southern margin of the Sauwald Zone, the S-type granite bodies of Schärding and Peuerbach occur (Thiele 1962). They intruded during a late stage of the regional anatexis and have been dated at ca. 315–320 Ma (Friedl 1997).

Most of the anatectic lithologies in the Sauwald Zone contain no mineral assemblages suitable for precise *P*–*T* estimates and consist of plagioclase + biotite + quartz ± K-feldspar ± cordierite. Exceptions are strongly peraluminous garnet + cordierite + sillimanite gneisses (metapelites or restites), which have been mapped as “Schiefergneise” in a few localities within the Sauwald Zone (Thiele 1962). Initially, these rocks were considered to be pre-Variscan gneisses with relict mineral assemblages (Thiele 1962; Fuchs and Thiele 1968). However, today it is mostly believed that they are also products of the late-Variscan low-*P*/high-*T* overprint (Frasl and Finger 1991), although this was never confirmed by geochronological data. With regard to its anatectic lithology, the Sauwald Zone of Austria can be well correlated with the Bavarian Forest (Troll 1964), which forms the northwest continuation of the Austrian Moldanubian Unit. Many rocks in the Bavarian Forest show evidence of a similar anatectic low-*P*/high-*T* overprint as well, as shown already by Schreyer et al. (1964), Schreyer and Blümel (1974) and Blümel and Schreyer (1976, 1977). In the course of their investigations, *P*–*T* conditions of 650–730°C and 0.2–0.4 GPa were determined for the anatectic low-*P*/high-*T* overprint. The most recent study on migmatites from this area was carried out by Kalt et al. (1999, 2000) in the area of Bodenmais, Bavarian Forest. They determined peak *P*–*T* conditions of ca. 850°C at 0.5–0.7 GPa, while the age of anatexis was constrained to be 323–326 Ma (U–Pb zircon and monazite ages). Similar monazite ages have previously been published from other locations in the Bavarian Forest (Grauert et al. 1974). It therefore seems that the late-Variscan low-*P*/high-*T* metamorphism in the Bavarian Forest and in the adjoining Sauwald Zone of Austria is significantly younger than the low-*P*/high-*T* metamorphism in the Monotonous unit east of the South Bohemian Batholith (334 ± 1 Ma).

Samples for the present study have been taken near the villages of Kößldorf and Pyret (Western Sauwald Zone; Fig. 1), where garnet-bearing gneisses have been mapped by Thiele (1962). Some mineral compositions and *P*–*T* estimates for the first-named locality have been briefly mentioned in conference abstracts of Knop et al. (1995, 2000), but have never been published so far in detail.

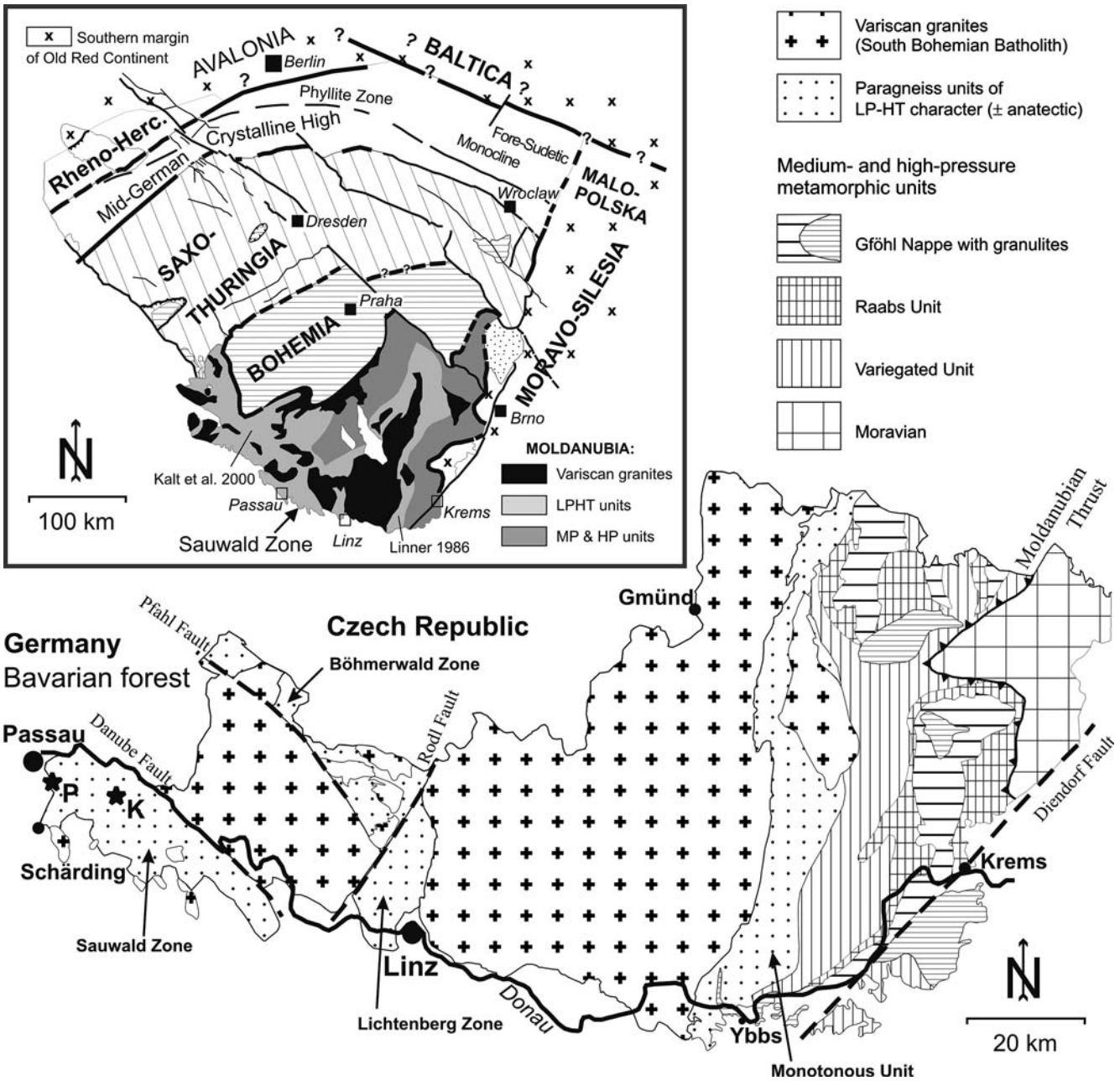


**Fig. 1** Simplified geological map of the Austrian part of the Bohemian Massif showing the major units with low-*P*/high-*T* metamorphism and the sample locations in the Sauwald Zone (*P* Pyret, *K* Kößldorf). Inset: Terrane map for the Bohemian Massif after Franke and Zelazniewicz (2000). Distribution of low-*P*/high-*T* and medium- and high-*P* metamorphic units in the Moldanubian slightly modified after O'Brien (2000)

## Petrography

The rocks of this investigation contain the mineral assemblage garnet + cordierite + spinel + sillimanite + K-feldspar + plagioclase + quartz + biotite + muscovite + magnetite + graphite + ilmenite + apatite + zircon which represents a succession of different growth stages during the metamorphic overprint, which will be discussed below (Table 1). Occasionally, small layers or lenses of leucocrate minerals (K-feldspar, plagioclase, quartz) occur, which might represent former partial melts (Fig. 2).

Garnet porphyroblasts range in size from less than 1 mm up to 4 mm and frequently occur as resorbed relics (Fig. 3a). Within garnets, inclusions of plagioclase, green spinel (Fig. 3b), quartz, ilmenite, sillimanite, cordierite, monazite, zircon (Fig. 3c) and biotite occur. Along the resorbed garnet rims, cordierite and K-feldspar occur (Fig. 3d). Sillimanite needles can be found as

**Table 1** Overall mineral assemblages of the samples

| Sample | Qtz | Grt | Bt | Rt | Chl | Pl | Kfs | Spl | Crd | Sill | Ms | Zrn | Ttn | Ilm |
|---|---|---|---|---|---|---|---|---|---|---|---|---|---|---|
| K1A | × | × | × | – | – | × | × | × | × | × | × | × | – | × |
| K1A2 | × | × | × | – | – | × | × | × | × | × | × | × | – | × |
| K1B | × | × | × | – | – | × | × | × | × | × | × | × | – | × |
| K1B2 | × | × | × | – | – | × | × | × | × | × | × | × | – | × |
| K3 | × | × | × | – | – | × | × | × | × | × | × | × | – | × |
| PY1 | × | × | × | – | – | × | × | – | – | – | × | × | – | × |
| PY3 | × | – | × | – | × | × | × | – | – | – | × | × | - | × |
| PY4 | × | – | × | – | × | × | × | – | – | – | × | × | – | × |
| PY5 | × | – | × | × |  | × | × | – | – | – | × | × | – | × |
| PY6 | × | – | × | – | – | × | × | – | × | – | – | × | – | × |
| PY8 | × | – | × | × | × | × | × | – | × | × | × | × | – | × |
| PY9 | × | – | × | – | × | × | × | × | – | – | × | × | × | × |
| PY10 | × | – | × | – | × | × | × | – | – | – | × | × | × | × |
| PY11 | × | × | × | – | – | × | × | × | × | × | × | × | – | × |
| PY12 | × | – | × | – | – | × | × | – | × | – | × | × | – | × |
| WE3A | × | – | × | × | × | × | × | – | × | – | × | × | – | × |
| WE3B | × | – | × | × | × | × | × | – | × | – | × | × | – | × |
| SCH2 | × | – | × | × | – | × | × | – | × | – | × | × | – | × |

Sample localities: *K* Kößldorf, *PY* Pyret, *WE* Wernstein, *SCH* Schärding. Mineral abbreviations after Kretz (1983)

inclusions in the cores of cordierite (Fig. 3e), spinel, biotite and garnet rims (Fig. 3f). Sillimanite also occurs as small needles in the matrix in both localities but in Kößldorf, very fine-grained sillimanite aggregates, which texturally appear to form later than the coarser needles, also occur (Fig. 3g). Fine-grained muscovite occurs in the matrix, either intercalated with biotite or as an alteration product of cordierite and feldspar. Biotite can be found as inclusions in garnet cores, as well as in biotite–muscovite intergrowths, biotite–quartz myrmekites (Fig. 3h) or as large matrix biotite flakes containing rutile needles. K-feldspar and plagioclase coexist in the matrix (Fig. 3i). Perthitic K-feldspar exhibits exsolution lamellae of albite. Plagioclase shows a chemical zonation with Ca-rich cores and Ca-poor rims (Fig. 3i). Spinel either occurs as brown, olive-green or dark green grains in the matrix, whereas only green spinel has been found as inclusions in garnet (Fig. 3b).

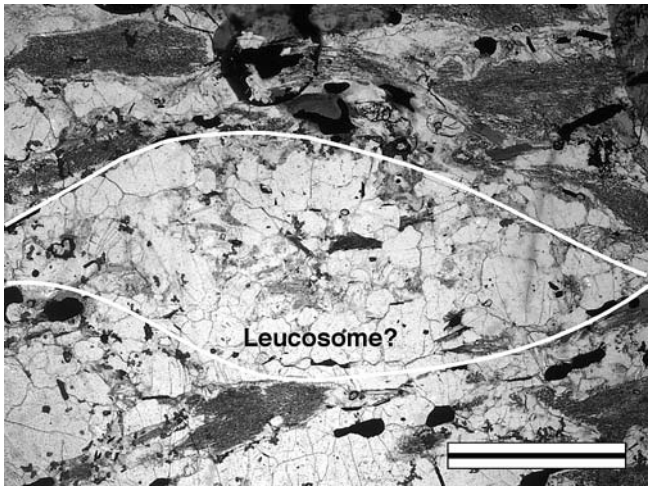


**Fig. 2** Photomicrograph of a leucocrate layer in a sample from Kößldorf. This layer mainly consists of K-feldspar + Plagioclase + Quartz and might represent a former leucosome (sample PY11). Length of scale bar is 0.5 mm

Based on textural observations, four stages of mineral growth could be discerned. The peak assemblage (stage 1), which occurs as an inclusion assemblage in garnet cores, is biotite + garnet core + green spinel + cordierite + sillimanite + plagioclase + quartz + ilmenite (Table 2). Within the matrix assemblage, we can distinguish between a post-peak1 (stage 2) and a post-peak2 (stage 3) assemblage based on the occurrence of spinel and sillimanite. Green spinel, garnet rim and cordierite cores with sillimanite inclusions together with plagioclase are thought to represent the stage 2 assemblage, whereas the assemblage olive-green and/or brown spinel, without sillimanite inclusions, plagioclase and the sillimanite-free cordierite rims form the stage 3 assemblage. Biotite seems to be stable throughout the whole metamorphic evolution. Late-stage (stage 4) features include K-feldspar growth at the rims of resorbed garnets (Fig. 3c), muscovite growing at the rims of biotite (Fig. 3g), fibrolite growing around coarser-grained sillimanite (Fig. 3f) and at the rims of biotite. Retrograde features also include albite growing around matrix plagioclase (Fig. 3h) and pinitisation of cordierite. Table 2 gives an overview of the four stages of mineral growth.

## Textural relations

Some of the textural relations can be related to the prograde and retrograde path and can be explained in terms of model reactions in the system $K_2O$–FeO–MgO–$Al_2O_3$–$SiO_2$–$H_2O$ (KFMASH).

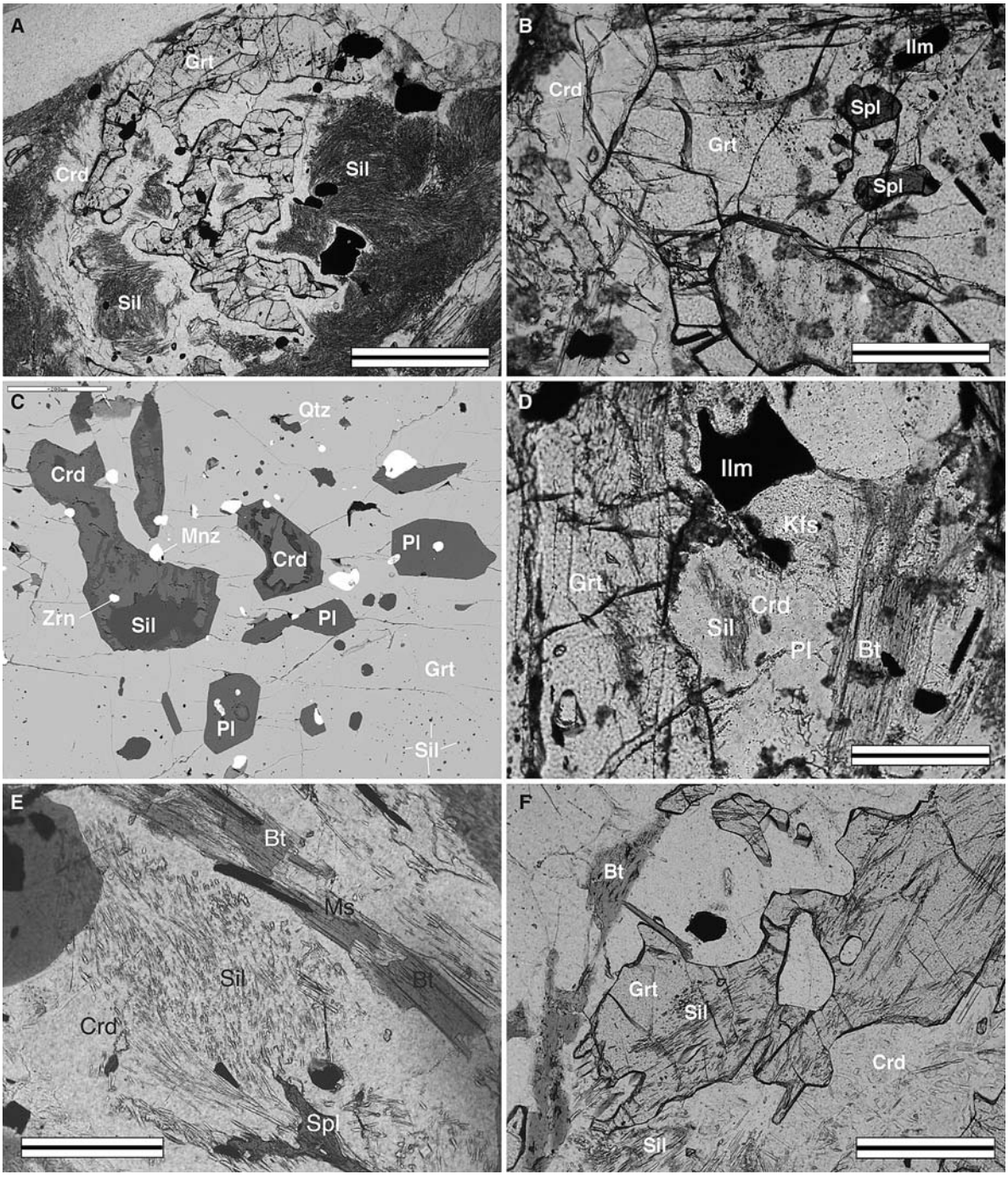


**Fig. 3** Photomicrographs and backscatter electron (*BSE*) images illustrating the textural relations in the samples. **a** Garnet (Grt) and sillimanite (Sil) being replaced by cordierite (Crd) in sample PY11. Length of scale bar is 0.5 mm. **b** Spinel (Spl) and ilmenite (Ilm) inclusions in garnet (Grt) in sample K1B. Along the garnet rim, cordierite (Crd) grows. Length of scale bar is 0.5 mm. **c** BSE image of the inclusion assemblage in a garnet core, namely An-rich plagioclase: Pl, cordierite (Crd), sillimanite (Sil), quartz (Qtz), zircon (Zrn) and monazite (Mz) in sample PY11. The *scale bar* represents 100 μm. **d** Garnet (Grt), sillimanite (Sil) and K-feldspar (Kfs) being replaced by cordierite (Crd) and biotite (Bt) in sample K1A. Ilmenite (Ilm) grows adjacent. Length of scale bar is 0.2 mm. **e** Matrix cordierite (Crd) with inclusions of sillimanite (Sil) and spinel (Spl) in sample K5. Biotite (Bt) shows late-stage growth of muscovite (Ms). Length of scale bar is 0.5 mm. **f** Garnet (Grt) and cordierite (Crd) showing sillimanite (Sil) inclusions in sample K5. Length of scale bar is 0.5 mm. **g** Two generations of sillimanite (Sil1: older, coarser-grained sillimanite, Sil2: younger fibrolitic sillimanite). Sil1 occurs as inclusions in cordierite (Crd) in sample K1B. Length of scale bar is 2 mm. **h** BSE image of muscovite–biotite intergrowths adjacent to cordierite (Crd), sillimanite (Sil) and K-feldspar (Kfs) in sample PY11. The *scale bar* represents 200 μm. **i** BSE image of feldspars (plagioclase: Pl, K-feldspar; Kfs and albite (Ab) adjacent to cordierite (Crd), sillimanite (Sil) and biotite (Bt) in sample K1A. Note the exsolution lamellae in K-feldspar. The *scale bar* represents 50 μm. All mineral abbreviations are according to Kretz (1983)

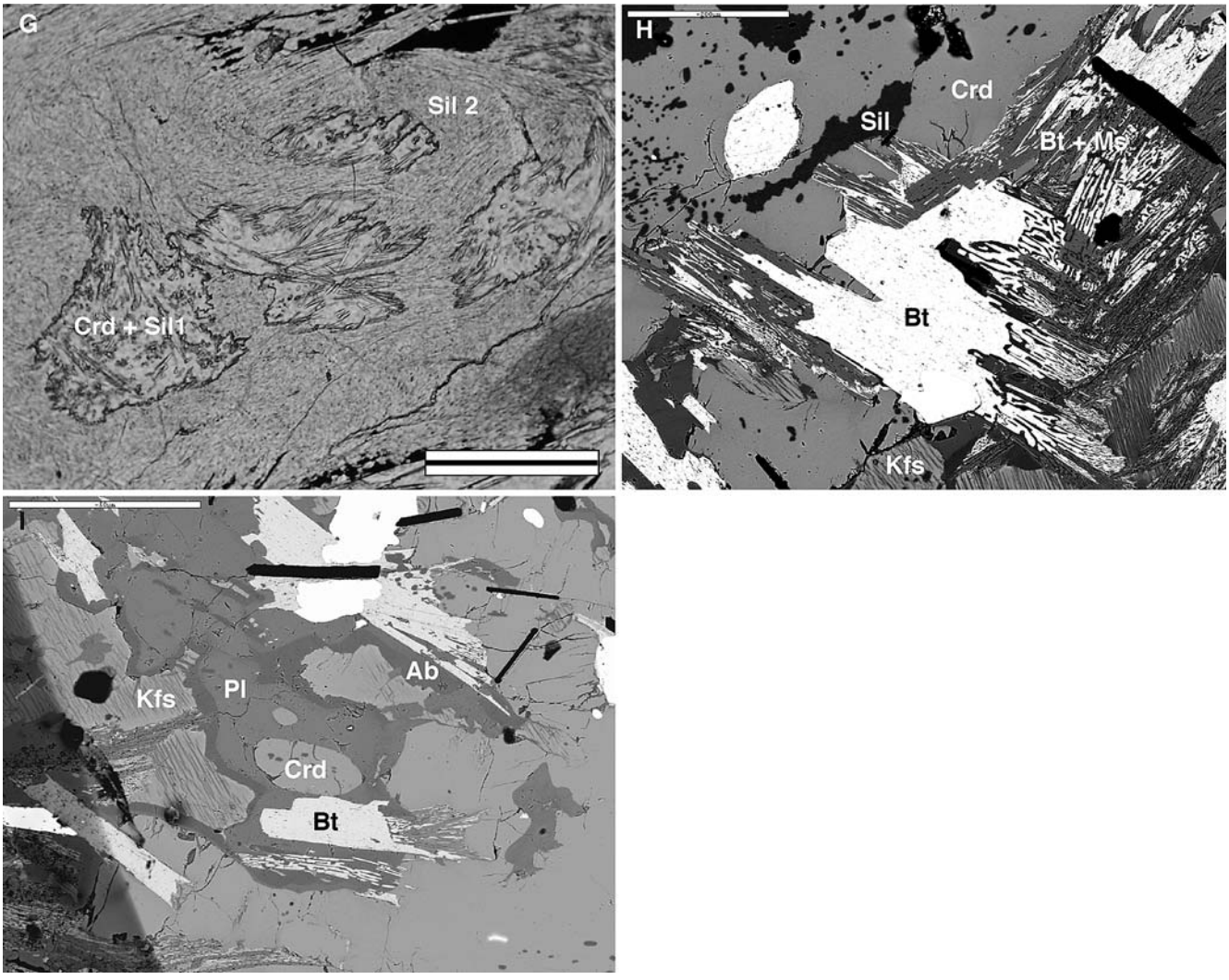


**Fig. 3** (Contd.)

Prograde path

Within cordierite, spinel and sillimanite inclusions occur (Fig. 3d), which could be due to the reaction:

$$\text{Biotite} + \text{Sillimanite} + \text{Quartz} = \text{Spinel} + \text{Cordierite} + \text{K-feldspar} + H_2O \quad (1)$$

Biotite, cordierite and sillimanite inclusions in garnet (Fig. 3c, f) also indicate the following reaction:

$$\text{Biotite} + \text{Sillimanite} = \text{Cordierite} + \text{Garnet} + \text{Melt}/H_2O \quad (2)$$

The absence of primary muscovite and the presence of K-feldspar porphyroblasts and sillimanite needles during the prograde evolution of these rocks suggests that the dehydration of primary muscovite according to reaction:

$$\text{Muscovite} + \text{Quartz} = \text{K- feldspar} + \text{Sillimanite} + \text{Quartz} + H_2O \quad (3)$$

already took place. The absence of orthopyroxene indicates that the *P–T* conditions did not exceed the thermal limit (e.g. dehydration breakdown) of the biotite stability field.

Retrograde path

Garnet is frequently resorbed and surrounded by cordierite, which contains sillimanite inclusions. This could be due to the continuous reaction:

$$\text{Garnet} + \text{Sillimanite} + \text{Quartz} = \text{Cordierite}. \quad (4)$$

Within these resorbed rims, K-feldspar and biotite also occur (Fig. 3d). This can be interpreted in terms of the reactions:

$$\text{Garnet} + \text{K-feldspar} + \text{Melt}/H_2O = \text{Cordierite} + \text{Biotite} \quad (5)$$

and

**Table 2** Mineral growth stages based on textural observations

| Mineral growth stage | Grt-inclusions (Peak) 1 | Matrix assemblage (Post-peak1) 2 | Matrix assemblage (Post-peak2) 3 | Late-stage and retrograde minerals 4 |
|---|---|---|---|---|
| Bt | ——— | ——— | ——— | ———?——— |
| Grt | ——— | ——— | | |
| Spl | ——Green spinel—— | ——Green spinel—— | -Olive/brown spinel- | |
| Crd | ——— | ——— | ——— | |
| Sil | ——— | ——— | | ———Fibrolite—— |
| Pl | ——— | ——— | ——— | ———Albite——— |
| Kfs | ——— | ——— | ——— | |
| Ms | | | | ——— |
| Qtz | ——— | ——— | ——— | |

All mineral abbreviations after Kretz (1983)

$$\text{Garnet} + \text{Sillimanite} + \text{Melt}/H_2O = \text{Cordierite} + \text{K-feldspar}. \quad (6)$$

The occurrence of fine sillimanite needles, growing seemingly later around coarser-grained sillimanite (Fig. 3f) and biotite, could indicate that the back-reaction of reaction 2 or the reaction

$$\text{Garnet} + \text{Cordierite} + \text{K-feldspar} + H_2O/\text{melt} = \text{Biotite} + \text{Sillimanite} + \text{Quartz} \quad (7)$$

took place in the rocks.

## Mineral chemistry

### Analytical techniques

Electron microprobe analyses of minerals were performed on an ARL—SEMQ microprobe in the Institute of Mineralogy and Petrography at the University of Innsbruck. The data were obtained with energy dispersive analysis (EDS) on a NORAN-Voyager EDS system, which was calibrated with synthetic elemental standards. The analytical conditions were 15 kV and a sample current of 20 nA on brass. The counting times ranged from 100 to 200 s. Most data were obtained with point mode, except for mica and feldspar, which were analyzed using a $10 \times 10$ μm rastered beam to prevent the volatilization of the alkalies. At the later stage of the investigation, only very few electron microprobe analyses of feldspar and cordierite were obtained on a JEOL 8100 Superprobe at the Institute of Mineralogy and Petrography at the University of Innsbruck. The analytical conditions were 10 kV and a sample current of 10 nA on brass. The counting times for most elements were 20 s for the peak and 10 s for the background, except for Na and K, which were analyzed with counting times of 100 s for the peak. Mineral formulae were then calculated with the programs MacAX (TJB Holland 1999, written communication) and NORM II (Ulmer 2002, written communication). Monazite analyses were performed on a JEOL JX 8600 in the Department of Geography, Geology and Mineralogy at the University of Salzburg. The analytical conditions for the JEOL JX 8600 microprobe in Salzburg were 15 kV and 200 nA beam current with long counting times of 240 s for Pb and 60 s for U. Further details of the analytical procedure are outlined in Finger and Helmy (1998).

Micro-Raman spectroscopy was performed on a Jobin-Yvon LabRAM-HR800 with a 633 nm He–Ne and a 325 nm He–Cd laser system in the Institute of Mineralogy and Petrology at the University of Graz.

*Garnet* is essentially an almandine-pyrope solid solution with minor ($< 4$ mol%) spessartine and grossular components (Table 3). Figure 4 shows a compositional profile through a large garnet porphyroblast from Kößldorf (K1B), which is zoned with grossular-rich cores and decreasing grossular- and pyrope- and increasing almandine contents toward the rims. In contrast, garnets from the sample locality Pyret show almost no zoning in Mg and Fe, but an occasional irregular distribution of Ca. Occasionally, resorbed garnet rims show a slight enrichment in the almandine component.

Although *Cordierite* shows optical zoning with sillimanite-rich cores and sillimanite-free rims, no obvious chemical zoning has been found in Fe, Mg and Na. The Mg# (Mg/Mg + Fe) ranges from 0.41 to 0.51 and indicates that cordierites roughly contain approximately equal amounts of Fe- and Mg-cordierite (Table 4). Cordierite inclusions show slightly higher Mg# of $0.51 \pm 0.004$ than cordierite cores and rims from the matrix ($0.46 \pm 0.03$). The Na contents are low and range from 0.021 to 0.029 Na a.p.f.u., and K contents are extremely low $< 0.01$ a.p.f.u. The analytical totals of 96–98 wt.% indicate the presence of channel components such as $H_2O$ and $CO_2$ in the cordierite structure. Since cordierites can contain up to 30% of channel components other than $H_2O$ and $CO_2$, such as Ar, $N_2$ and $CH_4$ (Aranovich and Podlesskii 1983), we used spectroscopic methods to make inferences about the nature of the channel components. In this investigation, we qualitatively determined the presence of $H_2O$ and $CO_2$ in its structure by micro-Raman spectroscopy. Raman spectroscopy of cordierite crystals in thin sections revealed the symmetric stretching mode of $CO_2$ in cordierite at a wave number of 1,383 $cm^{-1}$ (Fig. 5a), oriented parallel to the *x*-axis (Kolesov and Geiger 2000). The symmetric stretching mode of $H_2O$ in the cordierite structure occurs at 3,598 $cm^{-1}$ (Fig. 5b) and is

**Table 3** Representative electron microprobe analyses of garnet

| Analysis | 1 | 2 | 3 | 4 | 5 | 6 |
|---|---|---|---|---|---|---|
| $SiO_2$ | 37.00 | 36.50 | 36.74 | 36.21 | 36.54 | 36.66 |
| $Al_2O_3$ | 20.85 | 20.83 | 20.70 | 20.62 | 20.89 | 20.83 |
| $Fe_2O_3$ | 1.22 | 0.45 | 2.34 | 1.63 | 0.18 | 0.33 |
| FeO | 34.98 | 38.39 | 33.81 | 36.27 | 35.11 | 36.02 |
| MnO | 0.99 | 1.17 | 1.34 | 1.58 | 1.43 | 1.41 |
| MgO | 3.35 | 1.63 | 2.71 | 1.93 | 2.68 | 2.99 |
| CaO | 1.79 | 0.91 | 3.07 | 1.55 | 1.84 | 0.83 |
| Σ | 100.18 | 99.88 | 100.71 | 99.79 | 98.67 | 99.07 |
| Si | 2.975 | 2.983 | 2.950 | 2.957 | 2.988 | 2.989 |
| Al | 1.976 | 2.006 | 1.959 | 1.985 | 2.013 | 2.002 |
| $Fe^{3+}$ | 0.074 | 0.027 | 0.142 | 0.100 | 0.011 | 0.020 |
| $Fe^{2+}$ | 2.352 | 2.624 | 2.270 | 2.478 | 2.401 | 2.456 |
| Mn | 0.067 | 0.081 | 0.091 | 0.109 | 0.099 | 0.097 |
| Mg | 0.402 | 0.199 | 0.324 | 0.235 | 0.327 | 0.363 |
| Ca | 0.154 | 0.080 | 0.264 | 0.136 | 0.161 | 0.073 |
| Σ Cat. | 8.000 | 8.000 | 8.000 | 8.000 | 8.000 | 8.000 |
| Mg# | 0.146 | 0.070 | 0.125 | 0.087 | 0.120 | 0.129 |
| Grossular | 0.015 | 0.013 | 0.018 | n.d. | 0.048 | 0.014 |
| Almandine | 0.791 | 0.880 | 0.770 | 0.838 | 0.804 | 0.822 |
| Pyrope | 0.135 | 0.067 | 0.110 | 0.079 | 0.109 | 0.122 |
| Spessartine | 0.023 | 0.027 | 0.031 | 0.037 | 0.033 | 0.033 |
| Andradite | 0.037 | 0.014 | 0.072 | 0.046 | 0.005 | 0.010 |

Basis of formula calculation: 12 O and 8 cations; $Fe^{3+}$ was calculated based on charge balance considerations. 1 garnet core (K1-A), 2 garnet rim (K1-A), 3 garnet core (K1-B), 4 garnet rim (K1-B), 5 garnet core (PY11), 6 garnet rim (PY11), *n.d.* not detected

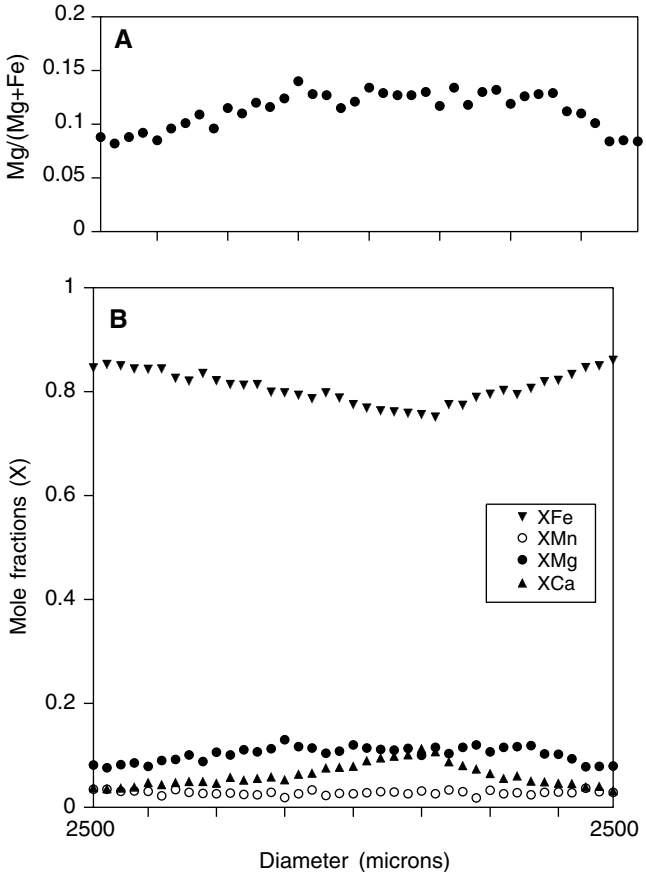


**Fig. 4** Compositional profile ($X_{Alm}$, $X_{Sps}$, $X_{Prp}$, $X_{Prp}$, $X_{Grs}$ and Mg#) through a garnet porphyroblast from sample K1B (Kößldorf); *reverse black triangle* $X_{Alm}$; *open circle* $X_{Sps}$; *black circle* $X_{Prp}$; *upright black triangle* $X_{Grs}$. The diameter of the garnet is 5 mm

diagnostic for class-I $H_2O$ molecules (Kolesov and Geiger 2000). Although the data are only qualitative (Kaindl et al. 2005 in preparation), the presence of $CO_2$ is in accordance with cordierite data from high-grade metamorphic rocks and shows that $a(H_2O)$ of the coexisting fluid phase will be $< 1$ (Vry et al. 1990; Harley et al. 2002).

### *Plagioclase*

Within plagioclases, three groups can be chemically distinguished based on their anorthite (An) contents (Table 5): (1) plagioclase inclusions in garnet show the highest An contents of 35–84 mol% An, where the highest An contents (55–84 mol%) occur in plagioclase inclusions in the core of large garnet porphyroblasts, (2) matrix plagioclase porphyroblasts show An contents of 10–45 mol% An and (3) albite rims around the matrix porphyroblasts show the lowest An contents of 0–15 mol% An (Fig. 6). Almost no K-feldspar component was detected in plagioclase.

*K-feldspar* is basically an albite—K-feldspar solid solution with albite (Ab) contents ranging from 10 to 15 mol% Ab component (Table 5). Most K-feldspars show perthitic exsolutions.

*Spinel* occurs in three variations, either as green, olive-green or brown spinel grains. Although all spinels are rich in hercynite component ($FeAl_2O_4$), these variations can also be chemically distinguished (Table 6). The chemical composition of spinels indicates a continuous solid solution, which mainly shows differences in the Zn and Cr contents as shown in Fig. 7. The Cr increases

**Table 4** Representative electron microprobe analyses of cordierite

| Analysis | 1 | 2 | 3 | 4 | 5 | 6 | 7 |
|---|---|---|---|---|---|---|---|
| $SiO_2$ | 47.04 | 47.13 | 47.12 | 46.71 | 47.28 | 47.41 | 47.31 |
| $Al_2O_3$ | 32.34 | 32.76 | 32.56 | 32.22 | 32.49 | 32.17 | 32.27 |
| FeO | 12.96 | 12.13 | 13.46 | 13.39 | 11.83 | 11.45 | 11.04 |
| MnO | n.d. | n.d. | 0.39 | n.d. | 0.27 | 0.14 | n.d. |
| MgO | 5.59 | 6.35 | 5.58 | 5.38 | 6.05 | 6.35 | 6.46 |
| $Na_2O$ | n.d. | n.d. | 0.21 | n.d. | 0.24 | 0.13 | n.d. |
| $K_2O$ | n.d. | n.d. | n.d. | n.d. | n.d. | n.d. | n.d. |
| $\Sigma$ | 97.93 | 98.37 | 98.94 | 97.70 | 98.16 | 97.65 | 97.08 |
| Si | 4.968 | 4.938 | 4.944 | 4.958 | 4.966 | 4.991 | 4.994 |
| Al | 4.026 | 4.046 | 4.025 | 4.030 | 4.022 | 3.992 | 4.015 |
| $Al^{IV}$ | 1.032 | 1.062 | 1.056 | 1.044 | 1.034 | 1.009 | 1.006 |
| $Al^{VI}$ | 2.994 | 2.984 | 2.969 | 2.988 | 2.988 | 2.983 | 3.008 |
| $Fe^{2+}$ | 1.145 | 1.063 | 1.181 | 1.189 | 1.039 | 1.008 | 0.975 |
| Mn | n.d. | n.d. | 0.000 | n.d. | 0.024 | 0.013 | n.d. |
| Mg | 0.880 | 0.992 | 0.872 | 0.851 | 0.947 | 0.996 | 1.016 |
| Na | n.d. | n.d. | 0.043 | n.d. | 0.049 | 0.027 | n.d. |
| K | n.d. | n.d. | n.d. | n.d. | n.d. | n.d. | n.d. |
| $\Sigma$ Cat. | 11.019 | 11.039 | 11.065 | 11.027 | 11.047 | 11.026 | 10.999 |
| Mg# | 0.435 | 0.483 | 0.425 | 0.417 | 0.477 | 0.497 | 0.510 |

Basis of formula calculation: 18 O + OH; 1 cordierite core (K1-A), 2 cordierite rim (K1-A), 3 cordierite rim (K1-B), 4 cordierite core (K1-B), 5 cordierite rim (PY11), 6 cordierite core (PY11), 7 cordierite inclusion in garnet core (PY11), *n.d.* not detected

from the green spinel continuously to the brown spinel, whereas Zn decreases. Overall, V shows no significant variation, but some spinels show considerable V contents of > 2 wt.% $V_2O_3$, indicating the presence of a small coulsonite component of < 0.03 mol%. Most spinels are chemically unzoned; only within the brown spinels, a slight increase of Cr was found toward the rims.

### *Biotite*

Three generations of biotite can be distinguished texturally and chemically by their $TiO_2$ contents: (1) relict biotite grains from the matrix and biotite inclusions in garnets show very high $TiO_2$ contents of up to 6.74 wt.% $TiO_2$ (Table 7); (2) matrix biotites contain 2–3 wt.% $TiO_2$ and (3) biotite from late-stage biotite–muscovite intergrowths show the smallest $TiO_2$ contents of less than 2 wt.% (Fig. 8).

### *Sillimanite*

Optically and chemically, two groups of sillimanites can be distinguished (Fig. 9). The texturally older, coarse-grained sillimanite crystals contain > 1 wt.% FeO, which corresponds to 0.024 a.p.f.u. $Fe^{3+}$, while the texturally younger, fine-grained fibrolite needles show smaller FeO contents of < 1 wt.% (0.01 a.p.f.u. $Fe^{3+}$).

*Muscovit*e only occurs in muscovite–biotite intergrowths as well as an alteration product in cordierite. The Si contents are very low (< 3.1 a.p.f.u.) as shown in Table 8.

## Thermobarometry

Thermobarometry was applied to three stages of mineral growth: (1) the metamorphic peak assemblage (stage 1): garnet (core) + cordierite (inclusion) + green spinel + sillimanite + plagioclase ($An_{35–65}$) + quartz; (2) the subsequent post-peak1 assemblage (stage 2): garnet (rim) + cordierite (matrix core) + green spinel + sillimanite + plagioclase ($An_{10–45}$) + quartz and (3) the retrograde stage involving muscovite formation (stage 4). The mineral assemblage used for estimating the peak metamorphic conditions occurs as inclusion in garnet cores. Calculations of *P–T* conditions of the subsequent post-peak1 assemblage involving the matrix assemblage were performed with the assemblage: garnet rim + sillimanite + cordierite core + plagioclase core + green spinel + biotite. The estimates of the retrograde stage involving muscovite formation were performed with the assemblage biotite + muscovite + K-feldspar + quartz. Thermobarometry was performed on a total of three samples (K1A, K1B and PY11) and chemical compositions of minerals from several domains within thin sections have been used for the calculations. K-feldspar has been excluded from calculations of the peak metamorphic conditions due to abundant albite exsolution lamellae.

### Garnet–cordierite–spinel–sillimanite thermobarometry

The *P–T* conditions of the peak (stage 1) assemblage garnet + cordierite + green spinel + sillimanite + quartz were calculated using the garnet–cordierite–spinel–sillimanite–quartz thermobarometry calibrated by Nichols et al. (1992). This thermobarometric technique considers all equilibria in the system FeO–MgO–$Al_2O_3$–$SiO_2$ (FMASH) among the assemblages garnet–spinel–sillimanite–quartz, cordierite–spinel–sillimanite–quartz and garnet–cordierite–sillimanite–quartz for thermobarometric calculations. Nichols et al. (1992) used the garnet activity model of Berman (1990), considered cordierite as an ideal solid solution and calibrated a ternary Fe–Mg–Zn symmetric mixing model for spinel. Application of the cordierite–spinel–sillimanite–quartz

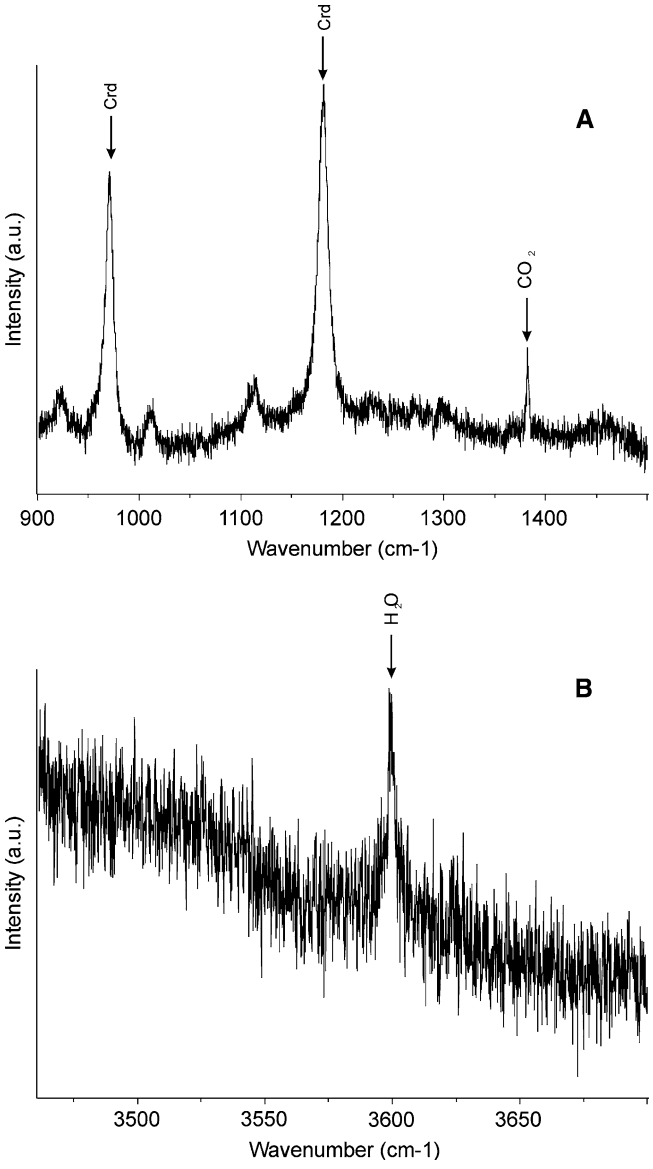


**Fig. 5** **a** Micro-Raman spectra showing the symmetric stretching mode of $CO_2$ at 1,383 $cm^{-1}$ and two internal $SiO_4$ stretching modes of cordierite at 973 and 1,185 $cm^{-1}$. **b** The symmetric stretching mode of $H_2O$ in cordierite at 3,598 $cm^{-1}$

thermobarometer to the peak assemblages in sample K1B from Kößldorf yields 0.35–0.51 GPa at temperatures of 750–800°C (Fig. 10). For samples K1A and K1B (Kößldorf), the garnet–cordierite–sillimanite–quartz thermobarometry yields 0.29–0.53 GPa at temperatures of 750–760°C and the garnet–spinel–sillimanite–quartz barometer yields pressures of 0.42–0.56 GPa at temperatures of 750–800°C for the peak metamorphic assemblage. Nichols et al. (1992) give uncertainties in the *P–T* estimates of 0.05–0.1 GPa and 50–100°C. Overall, the *P–T* estimates for the peak assemblage are 0.29–0.53 GPa and 750–800°C. Additional uncertainties in the *P–T* estimates by using the equilibria above result (1) from the unknown exact $H_2O$ and $CO_2$ contents of cordierite. Calculations in the dry (FAS, MAS) and $H_2O$-involving systems (FASH, MASH) represent only limiting *P–T* estimates. (2) The very small pyrope contents of garnet lie outside the range used in the garnet–cordierite–sillimanite–quartz calibration of Nichols et al. (1992).

## Inverse equilibrium thermobarometry (WEBINVEQ)

The WEBINVEQ uses given activities of the end-members of coexisting minerals and a least squares estimate of the pressure and temperature of the equilibration of a mineral assemblage. Instead of using a set of independent equilibria, *P* and *T* are defined by the best-fit hyperplane to the partial molar free energies of all phase components. The basic principles of the method are described by Gordon (1992), the thermodynamic database of *Berman* (1988, 1992 written communication) and the activity models by Berman (1990) for garnet, Fuhrman and Lindsley (1988) for plagioclase and McMullin et al. (1991) for biotite are used. For cordierite, an ideal ionic model was used which was calculated with the program MacAX (Holland 1999, written communication). Spinel contains significant amounts of ZnO and we used the activity model of Nichols et al. (1992) to account for non-ideal mixing involving Zn. With this method, we obtained pressures for the metamorphic peak (stage 1) assemblage garnet + cordierite + spinel

**Table 5** Representative electron microprobe analyses of feldspars

| Analysis | 1 | 2 | 3 | 4 | 5 | 6 |
|---|---|---|---|---|---|---|
| $SiO_2$ | 63.81 | 63.81 | 46.34 | 56.94 | 66.76 | 58.14 |
| $Al_2O_3$ | 18.69 | 18.72 | 33.91 | 26.43 | 19.92 | 25.82 |
| CaO | n.d. | n.d. | 17.41 | 8.37 | 0.42 | 7.76 |
| $Na_2O$ | 1.20 | 1.19 | 1.88 | 6.74 | 11.11 | 7.15 |
| $K_2O$ | 15.53 | 15.43 | n.d. | n.d. | n.d. | n.d. |
| Σ | 99.23 | 99.15 | 99.54 | 98.48 | 98.21 | 98.87 |
| Si | 2.955 | 2.958 | 2.133 | 2.585 | 2.974 | 2.625 |
| Al | 1.020 | 1.023 | 1.840 | 1.414 | 1.046 | 1.374 |
| Ca | n.d. | n.d. | 0.859 | 0.407 | 0.020 | 0.375 |
| Na | 0.108 | 0.107 | 0.168 | 0.593 | 0.960 | 0.626 |
| K | 0.917 | 0.912 | n.d. | n.d. | n.d. | n.d. |
| Σ Cat. | 5.000 | 5.000 | 5.000 | 5.000 | 5.000 | 5.000 |
| Albite | 11 | 11 | 16 | 59 | 97 | 63 |
| Anorthite | n.d. | n.d. | 84 | 41 | 3 | 37 |
| K-feldspar | 89 | 89 | n.d. | n.d. | n.d. | n.d. |

Basis of formula calculations: 8 O and 5 cations; 1 K-feldspar (K1-A), 2, K-feldspar (PY11), 3 plagioclase inclusions in garnet core (K1-A), 4 core of matrix plagioclase (K1-A), 5 albite rim around matrix plagioclase (PY11), 6 core of matrix plagioclase (PY11), *n.d.* not detected

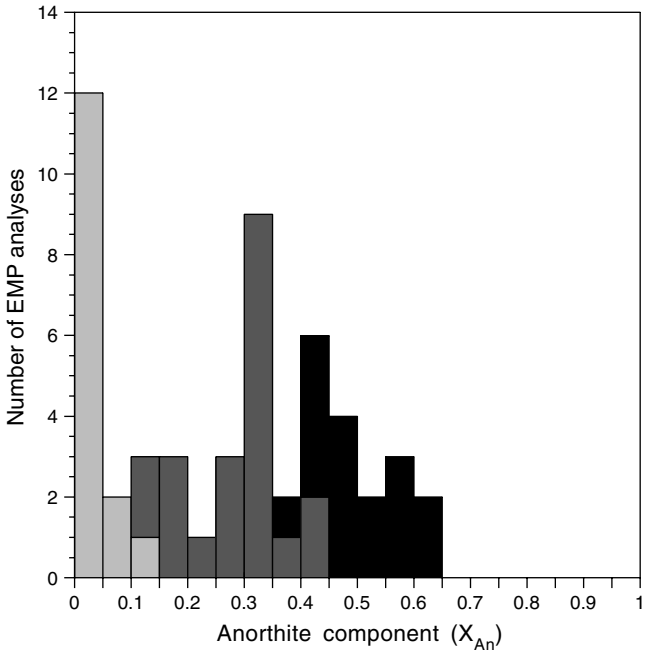


**Fig. 6** Compositional variation of feldspars from sample K1A; *black* plagioclase inclusions in garnet, *dark gray* cores and rims of matrix plagioclase, *light gray* late-stage albite rims around plagioclase

+ sillimanite + quartz of 790–810°C and 0.40 GPa for sample PY11 (Pyret) and 790–830°C and 0.35–0.37 GPa for sample K1B (Kößldorf) as shown in Table 9 and Figs. 11a, b. The *P–T* estimates for the matrix assemblage (post-peak1, stage 2) in samples K1A and K1B (Kößldorf) involving biotite give pressures of 0.27–0.36 GPa and temperatures of 620–730°C (Table 9; Fig. 11c, d). Since these calculations were performed with dry cordierite, they only provide limiting *P–T* estimates, but nonetheless are in good agreement with the *P–T* results by using the thermobarometric technique of Nichols et al. (1992), which also omits $H_2O$ from the calculations.

## Multi-equilibrium thermobarometry (THERMOCALC Version 3.1)

The simultaneous calculation of all possible reactions within a defined chemical system has been done by using the program THERMOCALC Version 3.1 (Table 10; Holland 2001, written communication) and the data set of Holland and Powell (1998). The approach we used is the average *P–T* calculation approach by Powell and Holland (1988, 1994). This approach utilizes calculation of all possible independent mineral reactions among a given set of minerals to obtain the equilibrium *P–T* conditions of the mineral assemblage. The natural composition of coexisting minerals is taken into account using the activity models for garnet, cordierite, plagioclase, muscovite and biotite from the program MacAX (Holland 1999, written communication). For spinel, we used the ternary model of Nichols et al. (1992). The activities were calculated initially at 0.4 GPa and 700°C. Subsequently, the determined conditions were used to re-calculate the activities again. This iteration process

**Table 6** Representative electron microprobe analyses of spinel

| Analysis | 1 | 2 | 3 | 4 | 5 | 6 | 7 | 8 | 9 | 10 |
|---|---|---|---|---|---|---|---|---|---|---|
| $TiO_2$ | n.d. | n.d. | 0.14 | n.d. | n.d. | n.d. | n.d. | n.d. | n.d. | 0.16 |
| $Cr_2O_3$ | n.d. | 0.28 | 6.41 | 2.46 | 3.58 | n.d. | 2.29 | 4.98 | 1.56 | 7.71 |
| $Al_2O_3$ | 56.66 | 56.90 | 50.37 | 53.30 | 52.42 | 55.91 | 54.02 | 51.07 | 55.06 | 49.16 |
| FeO | 36.61 | 35.86 | 34.24 | 36.07 | 36.12 | 34.79 | 35.50 | 33.77 | 34.30 | 34.40 |
| $Fe_2O_3$ | 1.91 | 2.03 | 1.58 | 2.54 | 2.49 | 3.16 | 2.39 | 2.84 | 1.82 | 1.75 |
| MnO | n.d. | n.d. | 0.29 | 0.34 | 0.26 | 0.28 | 0.17 | 0.60 | 0.20 | 0.40 |
| MgO | 1.51 | 1.62 | 1.73 | 1.07 | 1.34 | 1.37 | 1.22 | 1.28 | 1.83 | 1.52 |
| $V_2O_3$ | 0.36 | 0.31 | 0.93 | 0.81 | 0.71 | 0.32 | 0.52 | 2.15 | 0.52 | 1.40 |
| ZnO | 1.88 | 2.88 | 2.62 | 2.19 | 1.50 | 3.92 | 2.98 | 4.52 | 3.22 | 2.85 |
| $\sum$ | 98.93 | 99.87 | 98.31 | 98.77 | 98.42 | 99.75 | 99.09 | 101.20 | 98.51 | 99.34 |
| Ti | n.d. | n.d. | 0.003 | n.d. | n.d. | n.d. | n.d. | n.d. | n.d. | 0.004 |
| Cr | n.d. | 0.006 | 0.152 | 0.058 | 0.084 | n.d. | 0.053 | 0.116 | 0.036 | 0.183 |
| Al | 1.950 | 1.942 | 1.783 | 1.866 | 1.843 | 1.923 | 1.881 | 1.771 | 1.911 | 1.737 |
| $Fe^{2+}$ | 0.894 | 0.868 | 0.860 | 0.896 | 0.901 | 0.849 | 0.877 | 0.831 | 0.845 | 0.862 |
| $Fe^{3+}$ | 0.042 | 0.044 | 0.036 | 0.057 | 0.056 | 0.069 | 0.053 | 0.063 | 0.040 | 0.039 |
| Mn | n.d. | n.d. | 0.007 | 0.009 | 0.007 | 0.007 | 0.004 | 0.015 | 0.005 | 0.010 |
| Mg | 0.066 | 0.070 | 0.077 | 0.047 | 0.060 | 0.060 | 0.054 | 0.056 | 0.080 | 0.068 |
| V | 0.008 | 0.007 | 0.022 | 0.019 | 0.017 | 0.007 | 0.012 | 0.051 | 0.012 | 0.034 |
| Zn | 0.041 | 0.062 | 0.058 | 0.048 | 0.033 | 0.084 | 0.065 | 0.098 | 0.070 | 0.063 |
| $\sum$Cat. | 3.000 | 3.000 | 3.000 | 3.000 | 3.000 | 3.000 | 3.000 | 3.000 | 3.000 | 3.000 |
| $Fe_2TiO_4$ | n.d. | n.d. | 0.003 | n.d. | n.d. | n.d. | n.d. | n.d. | n.d. | n.d. |
| $FeV_2O_4$ | 0.004 | 0.004 | 0.011 | 0.010 | 0.008 | 0.004 | 0.006 | 0.025 | 0.006 | 0.005 |
| $MnFe_2O_4$ | n.d. | n.d. | 0.007 | 0.009 | 0.007 | 0.007 | 0.004 | 0.015 | 0.005 | n.d. |
| $ZnAl_2O_4$ | 0.041 | 0.062 | 0.058 | 0.048 | 0.033 | 0.084 | 0.065 | 0.098 | 0.070 | 0.032 |
| $FeCr_2O_4$ | n.d. | 0.003 | 0.076 | 0.029 | 0.042 | 0.000 | 0.027 | 0.058 | 0.018 | n.d. |
| $FeFe_2O_4$ | 0.021 | 0.022 | 0.010 | 0.020 | 0.021 | 0.028 | 0.022 | 0.016 | 0.015 | 0.021 |
| $MgAl_2O_4$ | 0.066 | 0.070 | 0.077 | 0.047 | 0.060 | 0.060 | 0.054 | 0.056 | 0.080 | 0.072 |
| $FeAl_2O_4$ | 0.869 | 0.840 | 0.756 | 0.838 | 0.829 | 0.817 | 0.822 | 0.731 | 0.805 | 0.870 |

Basis of formula calculation: 4 O and 3 cations; $Fe^{3+}$ was calculated based on charge balance considerations. 1, 2 green spinel (K1-A), 3 brown spinel (K1-A), 4 core of brown spinel (K1-B), 5 rim of brown spinel (K1-B), 6 green spinel (K1-B), 7 olive-green spinel (K1-B), 8 green spinel (PY11), 9 olive-green spinel (PY11), 10 brown spinel (PY11), *n.d.* not detected

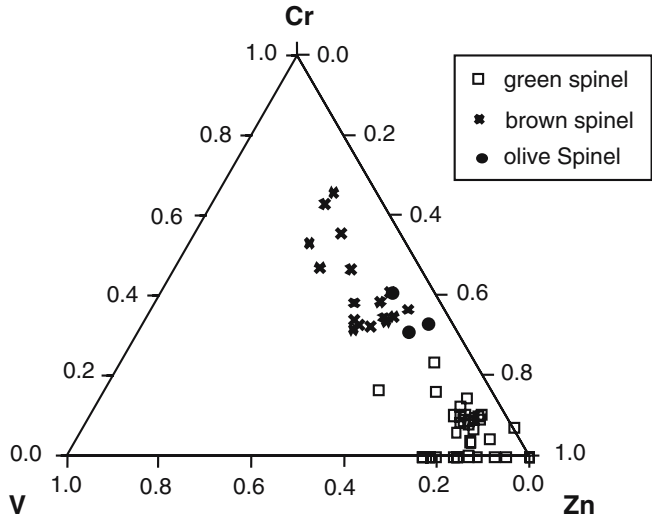


**Fig. 7** Ternary Cr-Zn-V diagram illustrating the chemical compositions of spinels in the Kößldorf samples (K1A and K1B)

was repeated until the data converged to less than 0.1 kbar and 10°C. The *P–T* conditions of the metamorphic peak (stage 1) assemblage garnet + cordierite + green spinel + sillimanite + quartz are, due to the involvement of cordierite, dependent on $a(H_2O)$. Therefore, the calculations were performed with variable $a(H_2O)$, assuming a binary $H_2O$–$CO_2$ fluid, namely $a(H_2O) = 0.9$, $a(H_2O) = 0.5$ and $a(H_2O) = 0.1$. Calculations with $a(H_2O) = 1$ have not been performed due to the verified presence of $CO_2$ in cordierite as outlined above. This yields *P–T* results for Kößldorf (K1A, K1B) ranging from 760–780°C and 0.4–0.55 GPa ($aH_2O = 0.9$) to 720°C and 0.3 GPa [$a(H_2O) = 0.1$] and for Pyret (PY11) ranging from 720–840°C and 0.4–0.55 GPa ($aH_2O = 0.9$) to 670–800°C and 0.3–0.4 GPa ($aH_2O = 0.1$). Due to the spread in the temperature estimates, it is impossible to infer $a(H_2O)$ from these calculations. On the other hand, varying $a(H_2O)$ between 0.9 and 0.1 only leads to a shift in pressure and temperature of about 0.15 GPa and 50°C, respectively.

## Cordierite thermobarometry

An important part of the evaluation of the *P–T*–$a(H_2O)$ conditions of these high-grade metapelites is the application of additional thermobarometric techniques involving cordierite. In recent years, an extensive evaluation of cordierite as a petrogenetic indicator in high-grade metapelites was performed (Mirwald and Knop 1995; Knop and Mirwald 1998; Mirwald 2000; Harley and Carrington 2001; Thompson et al. 2001, 2002; Harley et al. 2002). The studies of Knop and Mirwald (2000) and Thompson et al. (2002) focused on the incorporation of sodium in cordierite as a function of temperature, pressure and $a(H_2O)$. Mirwald (1986) and Knop and Mirwald (2000) found an inverse correlation between the sodium content and temperature, allowing the potential application of this relation as a thermometer. Their study also showed that the incorporation of sodium into cordierite is virtually pressure-independent. On the other hand, Thompson et al. (2002) performed the experiments in the presence of melt and observed a variation in $Na_2O$, which is an order of magnitude smaller than the results of Knop

**Table 7** Representative electron microprobe analyses of biotite

| Analysis | 1 | 2 | 3 | 4 | 5 | 6 |
|---|---|---|---|---|---|---|
| $SiO_2$ | 33.96 | 36.77 | 34.38 | 33.17 | 33.25 | 33.38 |
| $TiO_2$ | 6.74 | 2.15 | 1.76 | 5.68 | 2.55 | 1.70 |
| $Al_2O_3$ | 18.25 | 19.62 | 19.99 | 17.87 | 19.63 | 19.87 |
| $Cr_2O_3$ | 0.45 | n.d. | n.d. | n.d. | n.d. | n.d. |
| FeO | 23.50 | 21.58 | 22.77 | 23.45 | 25.29 | 23.90 |
| MnO | 0.53 | 0.30 | n.d. | n.d. | n.d. | n.d. |
| MgO | 4.78 | 6.02 | 6.38 | 6.15 | 5.37 | 5.75 |
| CaO | 0.12 | 0.16 | n.d. | n.d. | n.d. | n.d. |
| $Na_2O$ | 0.00 | 0.16 | n.d. | n.d. | n.d. | n.d. |
| $K_2O$ | 9.01 | 9.17 | 9.19 | 8.86 | 9.08 | 8.94 |
| $\sum$ | 97.34 | 95.93 | 94.47 | 95.18 | 95.17 | 93.54 |
| Si | 2.595 | 2.791 | 2.679 | 2.590 | 2.613 | 2.647 |
| Ti | 0.387 | 0.123 | 0.103 | 0.334 | 0.151 | 0.101 |
| Al | 1.644 | 1.755 | 1.836 | 1.644 | 1.818 | 1.857 |
| $Al^{IV}$ | 1.405 | 1.209 | 1.321 | 1.411 | 1.387 | 1.353 |
| $Al^{VI}$ | 0.239 | 0.547 | 0.515 | 0.234 | 0.431 | 0.504 |
| Cr | 0.027 | n.d. | n.d. | n.d. | n.d. | n.d. |
| $Fe^{2+}$ | 1.502 | 1.370 | 1.484 | 1.531 | 1.662 | 1.585 |
| Mn | 0.034 | 0.019 | n.d. | n.d. | n.d. | n.d. |
| Mg | 0.544 | 0.681 | 0.741 | 0.716 | 0.629 | 0.680 |
| Ca | 0.010 | 0.013 | n.d. | n.d. | n.d. | n.d. |
| Na | n.d. | 0.024 | n.d. | n.d. | n.d. | n.d. |
| K | 0.878 | 0.888 | 0.914 | 0.882 | 0.910 | 0.904 |
| $\sum$Cat. | 7.622 | 7.664 | 7.757 | 7.696 | 7.783 | 7.775 |
| Mg# | 0.266 | 0.332 | 0.333 | 0.319 | 0.275 | 0.300 |

Basis of formula calculation: 11 O; 1 Ti-rich biotite inclusion in garnet (PY 11), 2 core of matrix biotite (PY 11), 3 biotite analysis from muscovite–biotite intergrowths (PY 11), 4 Ti-rich biotite inclusion in garnet (K1-B), 5 core of matrix biotite (K1-A), 6 biotite analysis from muscovite–biotite intergrowths (K1-B), *n.d.* not detected

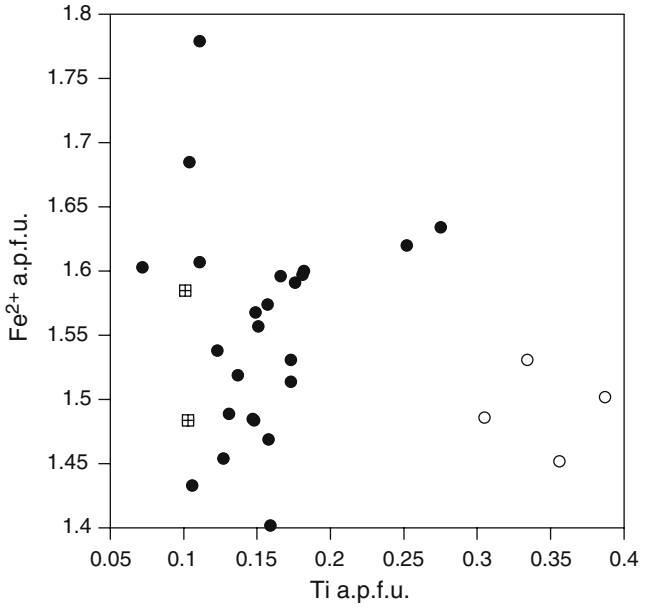


**Fig. 8** Fe versus Ti plot showing the biotite compositions from the Kößldorf samples K1A and K1B; *open circles* biotite inclusions in garnet, *black circles* matrix biotites, *cross-hatched squares* biotite analyses from muscovite–biotite intergrowths

**Table 8** Representative electron microprobe analyses of muscovite

| Analysis | 1 | 2 | 3 |
|---|---|---|---|
| $SiO_2$ | 47.09 | 47.48 | 45.49 |
| $TiO_2$ | n.d. | n.d. | 0.36 |
| $Al_2O_3$ | 37.62 | 35.50 | 36.18 |
| FeO | 1.05 | 1.35 | 0.86 |
| MgO | 0.47 | 0.32 | 0.32 |
| $Na_2O$ | 0.58 | 0.39 | 0.39 |
| $K_2O$ | 10.09 | 10.18 | 9.71 |
| $\sum$ | 96.90 | 95.22 | 93.31 |
| Si | 3.060 | 3.143 | 3.065 |
| Ti | n.d. | n.d. | 0.018 |
| Al | 2.881 | 2.769 | 2.873 |
| $Fe^{2+}$ | 0.057 | 0.075 | 0.049 |
| Mg | 0.046 | 0.032 | 0.032 |
| Na | 0.073 | 0.050 | 0.051 |
| K | 0.837 | 0.860 | 0.835 |
| $\sum$Cat. | 6.954 | 6.928 | 6.923 |

Basis of formula calculations: 11 O; 1 muscovite rims (K1-A), 2 muscovite core (K1-A), 3 muscovite from muscovite–biotite intergrowth (K-3), *n.d.* not detected

and Mirwald (2000). The reasons for this discrepancy are not clear yet. Knop and Mirwald (2000) and Scheikl and Mirwald (2000) showed that the sodium content of cordierite is also a monitor of the presence of fluid or melt in metapelitic rocks. Therefore, the sodium content of cordierites may serve as a monitor for $a(H_2O)$ as well as temperature in the rocks. Using the results from Knop and Mirwald (2000), our data indicate temperatures of ca. 650–700°C for cordierite in the subsolidus region in the presence of a fluid with $a(H_2O)$ ranging from 0.5 to 1.0. The Na content of cordierite in the presence of melt would indicate temperatures exceeding 850°C. Application of the Na-in - cordierite thermometer by Mirwald (1986) yields temperatures of ca. 770–800°C, which is closer to our previously obtained *P–T* estimates. Calculations of temperatures with the model of Thompson et al. (2002), assuming a fixed alkali composition of the melt (4.79 wt.% $K_2O$ and 4.37 wt.% $Na_2O$) as well as $a(H_2O)$ being low ($< 0.5$) yields temperatures ranging from 710 to 760°C. Although Kalt et al. (1999) showed that temperatures obtained with the formulation of Mirwald (1986) yielded consistent results in comparison with the results obtained with the garnet-biotite

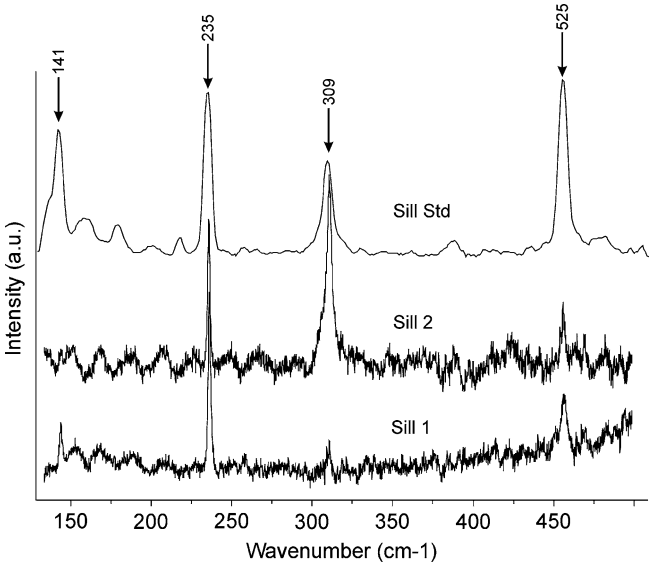


**Fig. 9** Background corrected micro-Raman spectra of sillimanite from samples K1A and K1B; *Sill*1 older coarser-grained sillimanite, *Sill*2 younger fibrolithic sillimanite, *Sill Std* sillimanite standard pattern

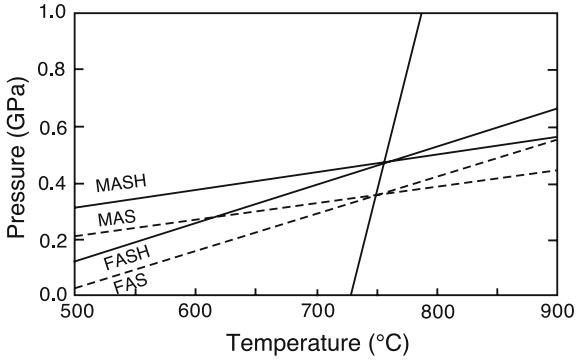


**Fig. 10** Results of the garnet–cordierite–sillimanite–quartz thermobarometry of sample K1B according to Nichols et al. (1992). The reactions illustrated in the systems FAS, FASH and MAS, MASH are: almandine + sillimanite = hercynite + quartz; pyrope + sillimanite + quartz = cordierite and pyrope + Fe – cordierite = almandine + cordierite

**Table 9** WEBINVEQ results

| Peak assemblage | Grt + Sill + Crd + Bt + Plag + Qz | | | |
|---|---|---|---|---|
| Sample | $P$ (GPa) | 1$\sigma$ | $T$ (°C) | 1$\sigma$ |
| PY11 | 0.40 | 0.049 | 814 | 74.7 |
| PY11 | 0.39 | 0.048 | 793 | 73.4 |
| PY11 | 0.39 | 0.048 | 787 | 73.1 |
| PY11 | 0.40 | 0.049 | 806 | 74.3 |
| Peak assemblage | Grt + Sill + Crd + Bt + Qz + Spl | | | |
| Sample | $P$ (GPa) | 1$\sigma$ | $T$ (°C) | 1$\sigma$ |
| K1B | 0.37 | 0.038 | 834 | 33.3 |
| K1B | 0.35 | 0.038 | 794 | 32.9 |
| Matrix assemblage | Grt + Sill + Crd + Bt + Plag + Qz + Spl | | | |
| Sample | $P$ (GPa) | 1$\sigma$ | $T$ (°C) | 1$\sigma$ |
| K1B | 0.32 | 0.038 | 729 | 32.4 |
| K1B | 0.31 | 0.037 | 697 | 27.9 |
| K1B | 0.28 | 0.037 | 656 | 31.4 |
| K1B | 0.29 | 0.037 | 678 | 27.7 |
| K1B | 0.30 | 0.038 | 691 | 31.9 |
| K1B | 0.30 | 0.037 | 686 | 27.7 |
| K1B | 0.31 | 0.092 | 721 | 34.9 |
| K1B | 0.36 | 0.090 | 761 | 35.8 |
| K1B | 0.36 | 0.091 | 679 | 33.2 |
| K1A | 0.30 | 0.037 | 655 | 27.4 |
| K1A | 0.30 | 0.038 | 673 | 32.2 |
| K1A | 0.29 | 0.037 | 647 | 27.5 |
| K1A | 0.28 | 0.038 | 624 | 31.5 |
| K1A | 0.27 | 0.037 | 620 | 27.0 |

thermometer, the investigations of Thompson et al. (2002) showed that additional variables such as the composition of the coexisting melt as well as an independent constraint on $a(H_2O)$ are necessary prerequisites when applying this thermometer to high-grade metamorphic rocks. Therefore, these results should only be viewed as additional qualitative temperature estimates.

The frequently observed assemblage cordierite + garnet + aluminiumsilicate + quartz in high-grade rocks can also be used as a geobarometer based on the divariant reaction

$$\text{(Mg, Fe)-cordierite} = \text{(Mg, Fe)-garnet} + \text{aluminiumsilicate} + \text{quartz} + H_2O \quad (8)$$

(Mirwald and Knop 1995). Using the Mg# of the garnet and cordierite cores yields pressures of ca. 0.45 GPa for temperatures of 750°C. Although cordierite-involving thermobarometry provides qualitative information, these data nonetheless provide independent $P$–$T$ estimates in addition to the thermobarometric estimates based on the methods presented above and are also in good agreement with the $P$–$T$ results of Knop et al. (2000), which yielded $P$–$T$ conditions of 780°C and 0.38 GPa.

### Thermobarometry involving late-stage muscovite-bearing assemblages

The late-stage muscovite–biotite intergrowths allow calculation of the empirical muscovite–biotite thermometer calibrated by Hoisch (1989). Figure 8 indicates that biotite from the muscovite–biotite intergrowths shows a chemical composition comparable with late-stage equilibration. This thermometer is based upon the tschermaks exchange between muscovite and biotite in the mineral assemblage muscovite + biotite + garnet + lagioclase + aluminium silicate + quartz. It gives temperatures of 530–570°C over a pressure range of 0.25–0.45 GPa. Retrograde overstepping of the reaction

$$\text{Celadonite} = \text{Biotite} + \text{K-feldspar} + \text{Quartz} + H_2O \quad (9)$$

to form late-stage muscovite yields limiting pressures of 0.2–0.4 GPa when calculated with THERMOCALC Version 3.1 and assuming $a(H_2O) = 1$. This pressure range is also in accordance with the Si-isopleths from the study of Massonne and Szpurka (1997).

## Monazite geochronology

One sample of garnet–cordierite gneiss (Fi-18/84) contains abundant monazite grains, which were analyzed with the electron microprobe to roughly constrain age data on the basis of Th–U–Pb chemical dating (Montel et al. 1996).

The analyzed monazites show a wide variation in their Th contents (4–18 wt.% $ThO_2$). The grains with the highest Th contents (grain 3 and 6 in Table 11) occur interstitially between quartz and feldspars and may have precipitated from a melt pocket, where Th can be strongly enriched (Watt 1995). All analyzed monazites have relatively low yttrium (1–2 wt.% $Y_2O_3$), probably due to their growth in an assemblage with garnet (Pyle et al. 2001), and because the host rock was undersaturated in $YPO_4$ at the given metamorphic conditions. The latter can be inferred from the lack of free xenotime.

The dating results are shown in Table 11 and Fig. 12. The ages cluster around a weighted average of 321 ± 9 Ma, suggesting that the low-$P$/high-$T$ metamorphism in the Sauwald Zone took place during a very late stage of the Variscan orgeny, close to the Visean/Namurian boundary. This age information is compatible with the ages of 323–326 Ma published by Kalt et al. (2000) for the peak of low-$P$/high-$T$ metamorphism in the Bavarian Forest. On the other hand, it is significantly younger than the monazite age of 334 ± 1 Ma given in Friedl (1997) for a paragneiss from the low-$P$/high-$T$ Monotonous Unit on the eastern side of the South Bohemian Batholith. This indicates that the low-$P$/high-$T$ metamorphism in the Austrian part of the Moldanubian Unit was not synchronous in all places.

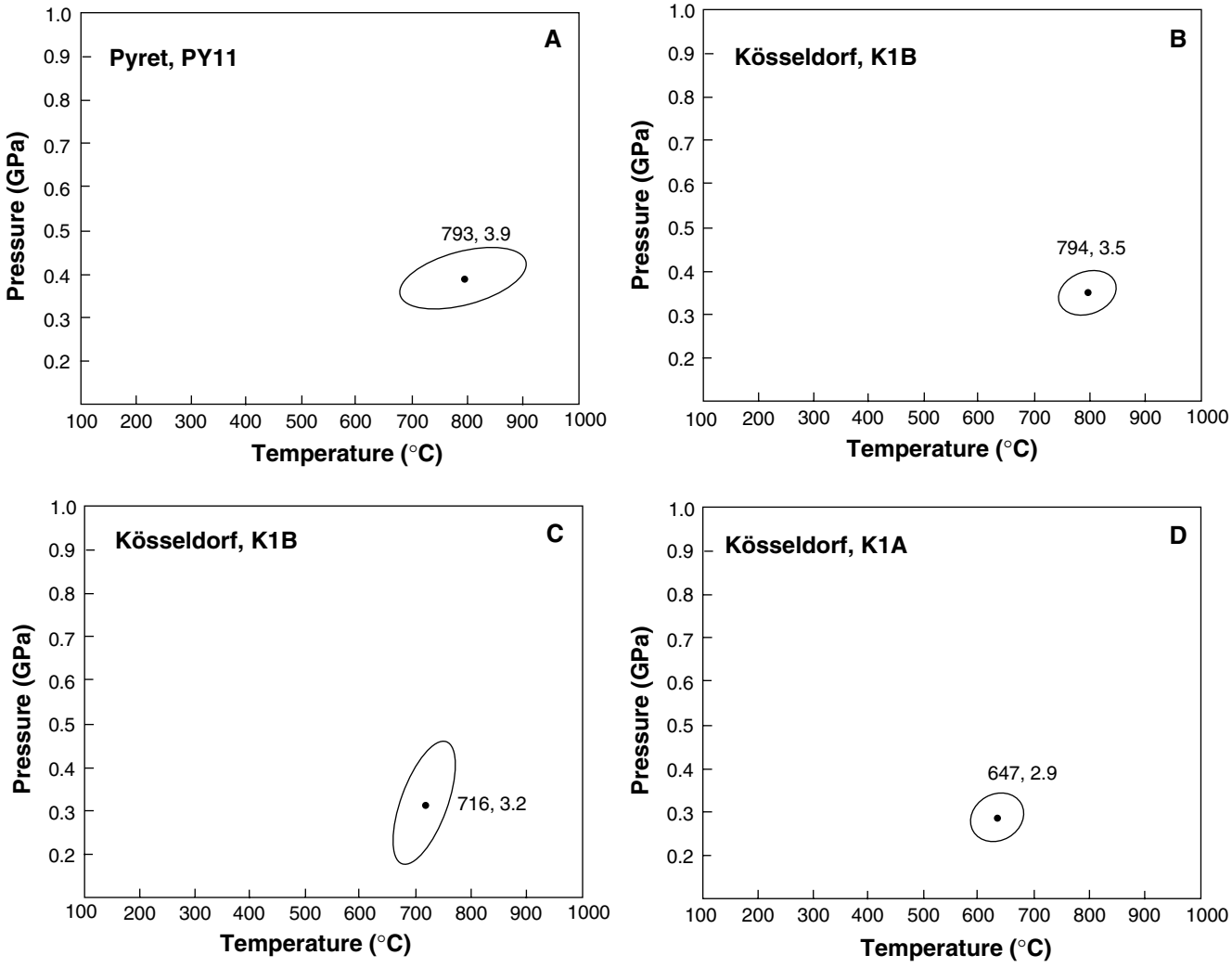


**Fig. 11** Results of the WEBINVEQ thermobarometry according to Gordon (1992). **a**, **b** *P–T* results of the metamorphic peak assemblage; **c**, **d** *P–T* results of the post-peak1 assemblage. The *solid ellipses* represent the *error ellipses* calculated according to Gordon (1992)

## Discussion

Petrological constraints on the *P–T* evolution of the granulites according to the petrogenetic grid of Spear et al. (1999)

Spear et al. (1999) presented a comprehensive overview of phase relations and mineral reactions in anatectic pelites with the mineral assemblage garnet + biotite + sillimanite + muscovite + quartz. The observed reaction textures and mineral zoning produced during partial melting provide important information about the *P–T* path of a metapelite sample (Fig. 13). Garnet and cordierite coexist and probably form through the reaction

$$\text{Biotite} + \text{Sillimanite} + \text{Quartz} = \text{Garnet} + \text{Cordierite} + \text{K-feldspar} + \text{H}_2\text{O/melt} \quad (10)$$

during the prograde *P–T* path. The prograde formation of spinel is probably the result of the reaction

**Table 10** THERMOCALC Version 3.1 results

| Sample | $a(H_2O) = 0.9$ | | | | $a(H_2O) = 0.5$ | | | | $a(H_2O) = 0.1$ | | | |
|---|---|---|---|---|---|---|---|---|---|---|---|---|
| | $T$ (°C) | 1$\sigma$ | $P$ (GPa) | 1$\sigma$ | $T$ (°C) | 1$\sigma$ | $P$ (GPa) | 1$\sigma$ | $T$ (°C) | 1$\sigma$ | $P$ (GPa) | 1$\sigma$ |
| K1B | – | – | – | – | – | – | – | – | 829 | 79 | 0.39 | 0.8 |
| K1B | 755 | 101 | 0.45 | 1.1 | 736 | 83 | 0.38 | 0.8 | 716 | 74 | 0.31 | 0.7 |
| K1A | 783 | 76 | 0.46 | 0.8 | 752 | 72 | 0.38 | 0.7 | 717 | 70 | 0.30 | 0.7 |
| PY11 | 723 | 89 | 0.40 | 0.9 | 699 | 85 | 0.33 | 0.8 | 670 | 80 | 0.25 | 0.7 |
| PY11 | 839 | 85 | 0.52 | 0.9 | 814 | 82 | 0.45 | 0.8 | 788 | 78 | 0.37 | 0.7 |
| PY11 | 842 | 92 | 0.55 | 1.0 | 823 | 91 | 0.48 | 0.9 | 798 | 92 | 0.39 | 0.8 |

**Table 11** Th, U and Pb contents and electron microprobe ages of monazites

| | Y | Th | U | Pb | Th* | Age (Ma) | 2σ |
|---|---|---|---|---|---|---|---|
| Mon 1 | 1.366 | 5.187 | 0.467 | 0.095 | 6.705 | 318 | 40 |
| Mon 2 | 1.345 | 4.725 | 0.697 | 0.102 | 6.991 | 328 | 39 |
| Mon 3 | 1.706 | 18.412 | 0.581 | 0.293 | 20.301 | 323 | 13 |
| Mon 4 | 1.206 | 7.511 | 0.421 | 0.122 | 8.879 | 308 | 30 |
| Mon 5 | 1.148 | 3.791 | 0.790 | 0.084 | 6.353 | 296 | 42 |
| Mon 6 | 1.728 | 11.321 | 0.670 | 0.194 | 13.499 | 321 | 20 |
| Mon 7 | 1.946 | 3.833 | 0.898 | 0.104 | 6.756 | 345 | 40 |
| | | | | | Mean | 321 | 9 |

Th, U and Pb contents. Th* values (Suzuki et al. 1991) and chemical ages (calculated after Montel et al. 1996) of monazites from sample Fi-18/84. Errors are 2σ for the single points and at the 95% confidence level for the weighted average age

biotite + illimanite = spinel + cordierite + K-feldspar + $H_2O$/melt. Our observed phase relations indicate heating along a clockwise *P–T* path into the stability field of the assemblage garnet + cordierite + spinel similar to path 3 of Spear et al. (1999).

Several chemical and textural features provide information about the retrograde part of the *P–T* path. During the retrograde portion of the *P–T* path, the Fe# in garnet increases due to the back reactions of the melt such as: garnet + K-feldspar + melt = cordierite + biotite and garnet + sillimanite + melt = cordierite + biotite, indicated by resorbed garnets and hence the late-stage growth of cordierite and biotite at the rims of some garnets. The rocks still contain abundant K-feldspar and minor retrograde muscovite, consistent with the clockwise *P–T* path 3 from Spear et al. (1999). It can be deduced that the rocks were cooled below the invariant point in the KASH system below 0.38 GPa as shown in Fig. 13.

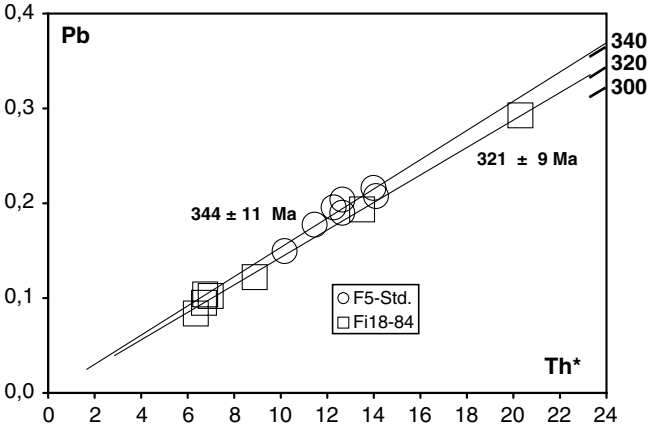


**Fig. 12** Total Pb versus Th* isochron diagram after Suzuki et al. (1991) using the values listed in Table 11. Time scale shown is based on the position of zero-intersect isochrons. Drawn isochrons refer to the calculated weighted average ages. A monazite age standard (F-5; recommended age 341 ± 2 Ma) was also measured to control the quality of the dating

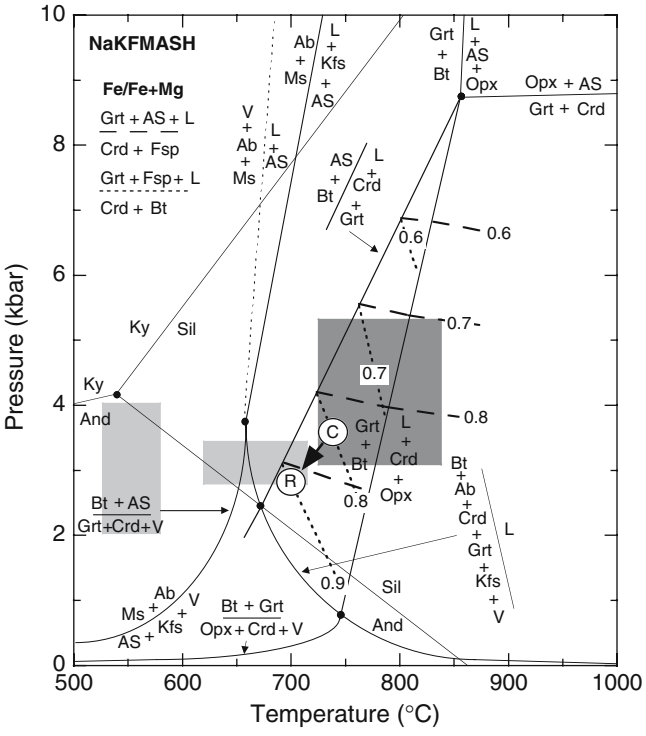


**Fig. 13** Petrogenetic grid in the system NaKFMASH from Spear et al. (1999) showing the metamorphic evolution of the metapelitic rocks from the Sauwald Zone. The dark gray square indicates peak *P–T* conditions, the medium gray box illustrates post-peak1 *P–T* conditions and the light gray box, *P–T* conditions of retrograde muscovite formation. The *dashed lines* indicate the isopleths of Fe# in garnet according the reaction garnet + sillimanite + melt = cordierite + K-feldspar, the *stipled line* indicates the the isopleths of Fe# in garnet according the reaction garnet + K-feldspar + melt = cordierite + biotite. The *circles* indicate garnet core (c) and garnet rim (r) compositions

## Geological implications for the late-Variscan evolution of the Moldanubian Unit

Compared to the *P–T* estimates published by Linner (1996) for the Monotonous Unit in Lower Austria, temperatures and the thermal gradient seem to be slightly higher in the Sauwald Zone, with peak *P–T* conditions of ca. 800°C at 0.3–0.5 GPa vs. 690–750°C and 0.4–0.5 GPa. These *P–T* conditions might even not represent peak conditions, since most of the rocks from the monotonous series contain no garnet. In addition, Linner (1996) put an upper constraint on the peak temperatures of ca. 800–820°C based on the lack of garnet in cordierite–biotite-bearing gneisses since the high-*T* reaction

$$\text{Biotite} + \text{Cordierite} + \text{Quartz} = \text{Garnet} + \text{K-feldspar} + H_2O/\text{melt} \quad (11)$$

has not yet been overstepped. Whether this slight difference in temperature is responsible for the diatectic stage of most paragneiss lithologies in the Sauwald Zone with rather massive, nebulitic granitoid fabric, in

contrast to the more schistose and layered gneiss texture of the Monotonous Unit due to less partial melting, is debatable.

An important point is that the monazite ages in the Sauwald Zone are clearly younger than those in the Monotonous Unit (321 ± 9 Ma vs. 334 ± 1 Ma). There are two possible geological interpretations for this: (1) heating of the crust occurred in both units at significantly different times (path 1 in Fig. 14), which would indicate that the late-Variscan low-*P*/high-*T* metamorphism in the Moldanubian Unit took place in two or even more steps, with probably different geotectonic causes, or (2) the low-*P*/high-*T* metamorphic overprint could have affected both areas more or less synchronously at ca. 335 Ma, but with a much longer duration of the thermal event in the Sauwald Zone (path 2 in Fig. 14). Geochronological data from Ar–Ar muscovite and biotite ages show that the Monotonous Unit was definitely in a cooling stage between 330 and 320 Ma with temperatures below 500°C (Scharbert et al. 1997). On the other hand, the ca. 320 Ma age of low-*P*/high-*T* metamorphism in the Sauwald Zone, as derived from monazite dating in this work, is independently strengthened by a recent SHRIMP study of Teipel et al. (2004), which was carried out on metaigneous rocks east of Passau. Metamorphic zircon rims considered as having formed during the low-*P*/high-*T* metamorphic event gave ages between 314 ± 4 and 326 ± 6 Ma. Mica cooling ages of below 300 Ma (Scharbert et al. 1997) imply that the Sauwald Zone subsequently experienced relatively slow cooling (Fig. 14).

The presently available geochronological data do not allow us to distinguish whether the prograde *T*–*t* evolution of the Sauwald Zone followed path 1 or 2 as shown in Fig. 14. However, there are some observations that would argue in favor of a long duration of metamorphism in the Sauwald Zone. (1) The low-*P*/high-*T* metamorphism in the Sauwald Zone was seemingly pervasive in nature, since no older relics have been found in any of the rocks of the present study. Here, it differs significantly from the Monotonous Unit, where relics of medium- or high-pressure mineral parageneses have been found repeatedly (Linner 1996; O'Brien 2000). (2) Furthermore, a long duration of high-*T* metamorphism and a long temporal exposure of the rocks to anatectic conditions could explain why most of the Sauwald Zone paragneisses exhibit particularly homogenous, granitoid textures. Therefore, long time annealing may have destroyed former gneissous textures.

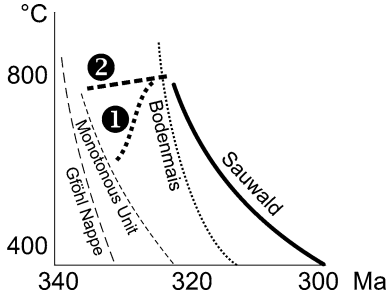


**Fig. 14** Sketch showing the approximate temperature–time evolution of different Moldanubian Units in Austria and the adjacent Bavarian Forest (Bodenmais area). The curves have been inferred from U–Pb ages of zircons and monazites (peak-*T* stage) and Ar–Ar hornblende and mica cooling ages published in the literature (Friedl 1997; Scharbert et al. 1997; Kalt et al. 2000; Teipel et al. 2004). For the prograde evolution of the Sauwald Zone, two possible *T*–*t* paths labeled 1 and 2 are discussed in the text

Our thermobarometric calculations yield *P*–*T* data for the Variscan low-*P*/high-*T* event (750–840°C, 0.29–0.53 GPa), which are significantly higher than previous estimates from the Bodenmais area by Schreyer and Blümel (1974) and Blümel and Schreyer (1976), which yielded 600–700°C and 0.2–0.3 GPa. The discrepancy simply lies in the thermodynamic data available at the time these investigations were performed, compared to the thermodynamic databases available today (e.g. Holland and Powell 1998), and the lack of activity-corrected *P*–*T* calculations at this time. Comparing our *P*–*T* data with those of Kalt et al. (1999) from the Bavarian forest (Bodenmais area, see Fig. 1), it would appear at first sight that the peak temperatures in the Sauwald Zone were slightly lower (800°C vs. 850°C), as were the pressures (0.3–0.5 GPa vs. 0.5–0.7 GPa). However, the peak temperature estimates of Kalt et al. (2000) may be somewhat too high, because (1) they rely on observed phase relations based on melting experiments by Vielzeuf and Montel (1994) and Stevens et al. (1997), carried out on material not fully analogous to the Bavarian Forest migmatites and (2) the highest temperatures in their study were obtained with the Na-in-cordierite thermometry, which was only empirically calibrated. On the other hand, most of their more robust thermombarometry yielded *P*–*T* results of 770–850°C and 0.44–0.51 Gpa, which were consistent with our data. It is important to note that, as was the case in the Sauwald Zone, orthopyroxene formation was not observed in the garnet–cordierite paragneisses investigated by Kalt et al. (2000), suggesting that the temperatures were probably not so much higher.

Regarding the timing of metamorphism in the Bavarian Forest (Bodenmais area), Kalt et al. (2000) concluded that the rocks were exposed to peak temperature conditions for a short period (max. 2.5 Ma at 850°C), and subsequently cooled at a moderate average cooling rate, reaching ca. 350°C at 310–315 Ma.

Even though the geochronological constraints presently available for the Sauwald Zone are of lower precision than those of Kalt et al. (2000) for the Bavarian Forest (Bodenmais area), it can be concluded that the *T*–*t* cooling path in the Sauwald Zone must have been more flat (Fig. 14), confirmed by biotite ages younger than 300 Ma (Scharbert et al. 1997). Thus, it can be speculated that the Sauwald Zone could have been situated immediately above a significant late-Variscan heat reservoir.

**Acknowledgments** Financial support through FWF-projects 12248 and 15133 (to F.F.) is gratefully acknowledged. Edgar Mersdorf is thanked for his assistance on the electron microprobe, and Gudrun Riegler for drawing the geological map and the *T-t* path. The discussions with Erich Knop at the initial stages of the project are greatly appreciated. Kurt Krenn is thanked for obtaining the additional micro-Raman spectra of cordierite. The constructive reviews of the journal reviewers Christoph Hauzenberger and Patrick O'Brien, as well as the editorial handling by Christian Dullo, are also greatly appreciated.

## References

Aranovich LYA, Podlesskii KK (1983) The cordierite–garnet–sillimanite–quartz equilibrium: experiments and applications. In: Saxena SK (ed) Kinetics and equilibrium in mineral reactions. Springer, Berlin Heidelberg New York, pp 173–198

Berman RG (1988) Internally-consistent thermodynamic data for minerals in the system $Na_2O$–$K_2O$–CaO–MgO–FeO–$Fe_2O_3$–$Al_2O_3$–$SiO_2$–$TiO_2$–$H_2O$–$CO_2$. J Petrol 29:445–522

Berman RG (1990) Mixing properties of Ca-Mg-Fe-Mn garnets. Am Mineral 75:328–344

Blümel P, Schreyer W (1976) Progressive regional low-pressure metamorphism in Moldanubian metapelites of the northern Bavarian Forest. Krystallinikum 12:7–30

Blümel P, Schreyer W (1977) Phase relations in pelitic and psammitic gneisses of the sillimanite-potash-feldspar and cordierite-potash-feldspar zones in the Moldanubicum of the Lam-Bodenmais area, Bavaria. J Petrol 18:431–459

Finger F, Clemens JD (1995) Migmatization and secondary granitic magmas: effects of emplacement and crystallization of primary granitoids in Southern Bohemia, Austria. Contrib Mineral Petrol 120:311–326

Finger F, Helmy HM (1998) Composition and total-Pb model ages of monazite from high-grade paragneisses in the Abu Swayel area, southern Eastern Desert, Egypt. Mineral Petrol 62:269–289

Finger F, Steyrer HP (1995) A tectonic model for the Eastern Variscides: indications from a chemical study of amphibolites in the south-eastern Bohemian Massif. Geol Carp 46:137–150

Finger F, Roberts MP, Haunschmid B, Schermaier A, Steyrer HP (1997) Variscan granites of central Europe: their typology, potential sources and tectonothermal relations. Mineral Petrol 61:67–96

Franke W (2000) The mid-European segment of the Variscides; tectonostratigraphic units, terrane boundaries and plate tectonic evolution. In: Franke W, Haak V, Oncken O, Tanner D (eds) Orogenic processes: Quantification and Modelling in the Variscan Belt. Geol Soc Spec Publ 179:35–61

Franke W, Zelazniewicz A (2000) The eastern termination of the Variscides: terrane correlation and kinematic evolution. In: Franke W, Haak V, Oncken O, Tanner D (eds) Orogenic Processes: Quantification and Modelling in the Variscan Belt. Geol Soc Lond Spec Publ 179:63–85

Frasl G, Finger F (1991) Geologisch-petrographische Exkursion in den österreichischen Teil des Südböhmischen Batholiths. Eur J Mineral Beih 3:23–40

Friedl G (1997) U/Pb-Datierungen an Zirkonen und Monaziten aus Gesteinen vom österreichischen Anteil der Böhmischen Masse. PhD Thesis, University of Salzburg, Austria, 242p

Friedl G, Finger F, Paquette JL, von Quandt A, McNaughton NJ, Fletcher IR (2004) Pre-Variscan geological events in the Austrian part of the Bohemian Massif deduced from U–Pb zircon ages. Int J Earth Sci (Geol Rundsch) 93:802–823

Fritz H, Dallmeyer RD, Neubauer F (1996) Thick-skinned versus thin-skinned thrusting: rheology controlled thrust propagation in the Variscan collision belt (the southeastern Bohemian Massif). Tectonics 15:1389–1413

Fuchs G, Matura A (1976) Zur Geologie des Kristallins der südlichen Böhmischen Masse. Jb Geol BA 119:1–43

Fuchs G, Thiele O (1968) Erläuterungen zur Übersichtskarte des Kristallins im westlichen Mühlviertel und im Sauwald, Oberösterreich. Geol Bundesanst Wien: 96p

Fuhrman ML, Lindsley DH (1988) Ternary feldspar modelling and thermometry. Am Mineral 73:201–216

Gerdes A, Wörner G, Henk A (2000) Post-collisional granite generation and HT-LP metamorphism by radiogenic heating: the Variscan South Bohemian Batholith. J Geol Soc London 157:577–587

Gerdes A, Friedl G, Parrish RR, Finger F (2003) High resolution geochronology of Variscan granite emplacement—the South Bohemian Batholith. J Czech Geol Soc 48:53

Gordon TM (1992) Solution of the inverse chemical equilibrium problem using data for individual species. Geochim Cosmochim Acta 56:1793–1800

Grauert B, Hanny R, Soptrajanova G (1974) Geochronology of a polymetamorphic and anatectic gneiss region: the Moldanubicum of the area Lam-Deggendorf, Eastern Bavaria, Germany. Contrib Mineral Petrol 45:37–63

Harley SL, Carrington DP (2001) The distribution of $H_2O$ between cordierite and granitic melt: $H_2O$ incorporation in cordierite and ist application to high-grade metamorphism and crustal anatexis. J Petrol 42:1593–1620

Harley SL, Thompson P, Hensen BJ, Buick IS (2002) Cordierite as a sensor of fluid conditions in high-grade metamorphism and crustal anatexis. J Metamorphic Geol 20:71–86

Henk A, von Blanckenburg F, Finger F, Schaltegger U, Zulauf G (2000) Syn-convergent high-temperature metamorphism and magmatism in the Variscides—a discussion of potential heat sources. Geol Soc Lond Spec Publ 179:387–399

Hoisch TD (1989) A muscovite–biotite geothermometer. Am Mineral 74:565–572

Holland TJB, Powell R (1998) An internally-consistent thermodynamic data set for phases of petrological interest. J Metamorphic Geol 16:309–343

Kalt A, Berger A, Blümel P (1999) Metamorphic evolution of cordierite-bearing migmatites from the Bayrische Wald (Variscan Belt, Germany). J Petrol 40:601–627

Kalt A, Corfu F, Wijbrans JP (2000) Time calibration of a *P–T* path from a Variscan high-temperature low-pressure complex (Bayrische Wald, Germany) and the detection of inherited monazite. Contrib Mineral Petrol 138:143–163

Klötzli US, Parrish RR (1996) Zircon U/Pb and Pb/Pb geochronology of the Rastenberg granodiorite, South Bohemian Massif, Austria. Mineral Petrol 58:197–214

Knop E, Mirwald PW (1998) Sodic cordierites: comparison of natural data and incorporation experiments. Mitt Österr Mineral Ges 143:316–321

Knop E, Mirwald PW (2000) Cordierite as a monitor of fluid and melt sodium activity in metapelites, migmatites and granites: constraints from incorporation experiments. J Conf Abstr 5:58

Knop E, Büttner S, Haunschmied B, Finger F, Mirwald P (1995) *P–T*-conditions of Variscan metamorphism and migmatization in the Sauwald, Southern Bohemian Massif. Terra Nova 7, Abstr Suppl 1:316

Knop E, Tropper P, Finger F (2000) The *P–T–a*($H_2O$) Path of migmatites from the sauwald, southern Bohemian Massif: comparison between predicted and observed textural relations in migmatites. Eur J Mineral Beih 12:98

Kolesov BA, Geiger CA (2000) Cordierite II: the role of $CO_2$ and $H_2O$. Am Mineral 85:1265–1274

Kretz R (1983) Symbols for rock-forming minerals. Am Mineral 68:277–279

Linner M (1996) Metamorphism and partial melting of paragneisses of the Monotonous Group, SE Moldanubicum (Austria). Mineral Petrol 58:215–234

Massonne HJ, Szpurka Z (1997) Thermodynamic properties of white micas on the basis of high-pressure experiments in the systems $K_2O$–MgO–$Al_2O_3$–$SiO_2$–$H_2O$ and $K_2O$–FeO–$Al_2O_3$–$SiO_2$–$H_2O$. Lithos 41:229–250

McMullin DWA, Berman RG, Greenwood HJ (1991) Calibration of the SGAM thermobarometer for pelitic rocks using data from phase equilibrium experiments and natural assemblages. Can Mineral 29:889–908

Mirwald PW (1986) First cordierit ein geothermometer. Fortschr Mineral 64:119

Mirwald PW (2000) The incorporation of $H_2O$ and $CO_2$ in cordierite at varying sodium content under subsolidus conditions. Eur J Mineral Beih 12:128

Mirwald PW, Knop E (1995) Der Einfluß der Kanalkomponenten $H_2O$, $CO_2$ und $Na^+$ auf die oberste Stabilität von Mg–Cordierit—eine experimentelle Pilotstudie und ihre Bedeutung für das Granat–Cordierit-Geobarometer. Geol Paläont Mitt Innsbruck 20:153–164

Montel JM, Foret S, Veschambre M, Nicollet CH, Provost A (1996) A fast, reliable, inexpensive in-situ dating technique: electron microprobe ages on monazite. Chem Geol 131:37–53

Nichols GT, Berry RF, Green DH (1992) Internally consistent gahnitic spinel–cordierite–garnet equilibria in the FMASHZn system: geothermobarometry and applications. Contrib Mineral Petrol 111:362–377

O'Brien PJ (2000) The fundamental Variscan problem: high-temperature metamorphism at different depths and high-pressure metamorphism at different temperatures. Geol Soc London Spec Publ 179:369–386

Powell R, Holland TJB (1988) An internally consistent thermodynamic dataset with uncertainties and correlations: III: application methods, worked examples and a computer program. J Metamorphic Geol 6:173–204

Powell R, Holland TJB (1994) Optimal geothermometry and geobarometry. Am Mineral 79:120–133

Pyle JM, Spear FS, Rudnick RL, Mc Donough WF (2001) Monazite–xenotime–garnet equilibrium in metapelites and a new monazite–garnet thermometer. J Petrol 42:2083–2107

Scharbert S, Breiter K, Frank W (1997) The cooling history of the southern Bohemian Massif. J Czech Geol Soc 42/3:24

Scheikl M, Mirwald PW (1999) Experimente zum Einfluß von Mischfluiden ($Na^+$, $CO_2$, und $H_2O$) auf die obere Druckstabilität von Mg- und Fe-Cordierit. Eur J Mineral Beih 11:198

Scheikl M, Mirwald PW (2000) The influence of different $H_2O$–$CO_2$ fluid compositions and Na-component on the P–T stability of Fe–cordierite. J Conf Abstr 5:91

Schreyer W, Blümel P (1974) Progressive metamorphism in the Moldanubian of the Northern Bavarian Forest. Fortschr Mineral 52:154–165

Schreyer W, Kullerud G, Ramdohr P (1964) Metamorphic conditions of ore and country rock of the Bodenmais, Bavaria, sulfide deposit. N Jb Mineral Abh 101:1–26

Spear FS, Kohn M, Cheney JT (1999) P–T paths from anatectic pelites. Contrib Mineral Petrol 134:17–32

Stevens G, Clemens JD, Droop G (1997) Melt production during granulite-facies anatexis: experimental data from primitive metasedimentary protoliths. Contrib Mineral Petrol 128:352–370

Suzuki K, Adachi M, Tanaka T (1991) Middle Precambrian provenance of Jurassic sandstone in the Mino Terrane, central Japan: Th–U–total Pb evidence from an electron microprobe monazite study. Sediment Geol 75:141–147

Teipel U, Eichhorn R, Loth G, Rohrmüller J, Höll L, Kennedy A (2004) U-PbSHRIMP and Nd isotopic data from the western Bohemian Massif (Bayerischer Wald, Germany): implications for Upper Vendian and Lower Ordovician magmatism. Int J Earth Sci 93:782–801

Thiele O (1962) Neue geologische Erkenntnisse aus dem Sauwald (O-Ö). Verh Geol BA 1962:117–129

Thompson P, Harley SL, Carrington DP (2001) $H_2O$–$CO_2$ partitioning between fluid, cordierite and granitic melt at 5 kbar and 900°C. Contrib Mineral Petrol 142:107–118

Thompson P, Harley SL, Carrington DP (2002) Sodium and potassium in cordierite—a potential thermometer for melts? Eur J Mineral 14:459–469

Troll G (1964) Geologische Übersichtskarte des Bayerischen Waldes 1:100.000. Geol Bav 58

Vielzeuf D, Montel JM (1994) Partial melting of metagreywackes. I. Fluid-absent experiments and phase relationships. Contrib Mineral Petrol 117:375–393

Vry JK, Brown PE, Valley JW (1990) Cordierite volatile content and the role of $CO_2$ in high-grade metamorphism. Am Mineral 75:71–88

Watt GR (1995) High-thorium monazite-(Ce) formed during disequilibrium melting of metapelites under granulite-facies conditions. Min Mag 59:735–743

Winchester JA, Pharaoh TC, Verniers J (2002) Palaeozoic Amalgamation of Central Europe. An introduction and synthesis of new results from recent geological and geophysical investigations. In: Winchester JA, Pharaoh TC, Verniers J (eds) Palaeozoic Amalgamation of Central Europe. Geol Soc Lond Spec Publ 201:1–18

Zwart HJ, Dornsiepen UF (1978) The tectonic framework of central and western Europe. Geol Mijnbow 57:627–654